MODELING OF NONLINEAR ELASTIC STRUCTURES USING MSC/NASTRAN

By

Ken Blakely and William B. Walton
ANCO Engineers, Inc.
Culver City, California

ABSTRACT

There are numerous structures that contain nonlinear elastic elements. Such elements possess nonlinear force-deflection relationships, yet they are elastic since they load and unload along the same force-deflection curve. Representing nonlinear elastic behavior can be accomplished using the pseudo-force procedure for which the system stiffness matrix remains unchanged, and the deviations from linearity are treated as additional applied loads. This approach, utilizing the MSC/NASTRAN NOLIN1 dynamic load in the linear transient analysis procedure, is computationally no more expensive than is a comparable, purely linear analysis.

Nonlinear elastic elements are described for actual structures. Then, the theory behind the pseudoforce technique is briefly discussed. Next, two large (several hundred degrees-of-freedom) sample problems are presented: in the first, base motion is applied to a structural system supported by nonlinear rubber shock isolators; in the second, snapback and high-level seismic excitations are applied to a piping system supported by nonlinear hangers. Results from the snapback simulations are compared to experimental measurements, and inclusion of the nonlinear supports is shown to more accurately reproduce the test data than does an equivalent linear model. Finally, some considerations are given in regard to modeling techniques and time step selection for analyzing nonlinear elastic structures via the pseudoforce approach.

INTRODUCTION

There are numerous structures that contain nonlinear elastic elements. These elements possess nonlinear force-deflection relationships, yet they are elastic since they load and unload along the same force-deflection curve (and therefore do not exhibit hysteresis). Examples of nonlinear elastic force-deflection curves are shown in Figure 1. These types of elements are common in many mechanical and structural systems, including: piping systems supported by nonlinear springs, chains (stiffness in tension only), or constant force devices; base-mounted equipment and structure supported by nonlinear shock isolation systems; structures with gaps (piping systems and buildings); and soil or concrete structures, which only exhibit stiffness when in compression. Other systems exhibit nonlinearities that are proportional to the rate of displacement (such as seat belts and snubbers

Accurate simulation of such nonlinearities is important for accurate representation of structures containing these nonlinear elastic systems. The next section describes several ways in which nonlinear elastic systems can be modeled in MSC/NASTRAN, with emphasis on the efficient pseudoforce method. Following that are two examples for which the pseudoforce method was used; the first example represents a 700 degree-of-freedom (DOF) turbine structure supported by nonlinear shock isolators, and the second example represents a 774 DOF piping system supported by bilinear springs. General discussion of the pseudoforce method is presented at the end of the text. Concluding the paper is an appendix that presents an extensive validation of the pseudoforce method.

METHODS OF SOLUTION

There are several methods in MSC/NASTRAN for solving nonlinear elastic problems [1,2]*. A general nonlinear solution scheme (SOL 99) could be used, in which the material properties would be specified as nonlinear elastic

*Numbers in brackets denote references.

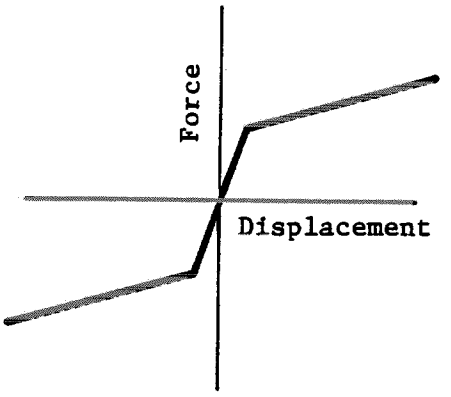

a. Bilinear spring

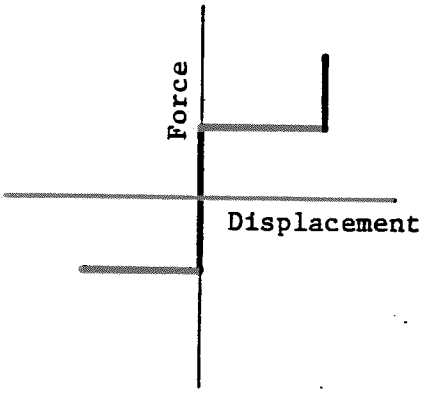

b. Preloaded constant force device, with hard stop

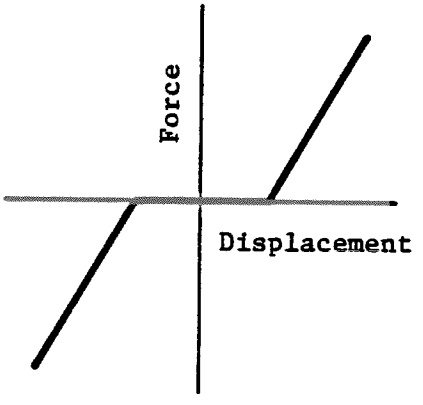

c. Gap and spring in series

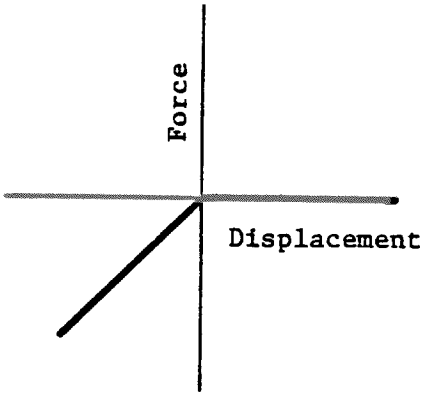

d. Stiffness in compression only

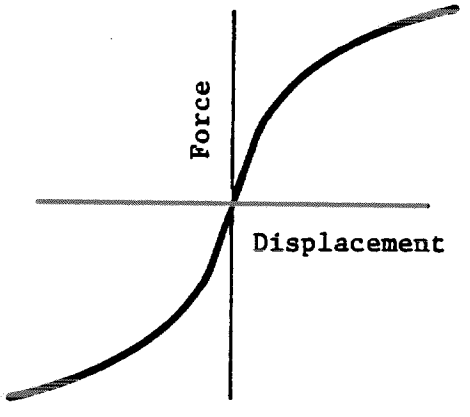

e. Softening system

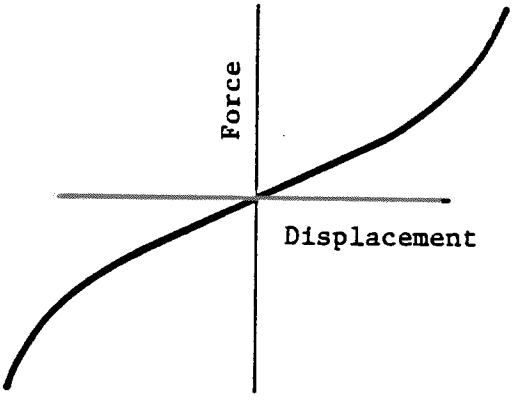

f. Hardening system

Figure 1: Examples of Nonlinear Elastic Systems

(NLELAST on the MATS1 card). Nonlinear element stiffness matrices would be generated, and equilibrium iterations and convergence checks would be required at each load step. In addition, gap elements (CGAP) could be used in conjunction with elastic elements to produce systems with piecewise linear force-deflection curves. This, too, would require the additional computations of nonlinear element stiffness matrix generation, equilibrium iteration, and convergence testing. Nonlinear analyses requiring these additional computations can be substantially more costly than an equivalent linear analysis, even if the nonlinearities are relatively few in number.

An efficient technique--the pseudoforce method-- exists in MSC/NASTRAN, in which localized nonlinearities are treated in such a manner as to require no additional computer time as compared to a purely linear analysis. In this method, which is available only for transient solutions, deviations from linearity are treated as additional applied loads. The dynamic equations of motion are written as

$$[M]\{\ddot{x}(t)\} + [C]\{\dot{x}(t)\} + [K]\{x(t)\} = \{f(t)\} + \{n(t)\} \qquad (1)$$

where [M], [C], and [K] denote the system mass, damping, and stiffness matrices, respectively. The vectors {f(t)} and {x(t)} denote applied nodal loads and system displacements, respectively, as functions of time. Time derivatives are denoted by the "." symbol. The vector {n(t)} denotes the nonlinear forces, which are added to the right-hand side of Eq. 1 (and, hence, are treated as additional applied loads).

Implementation of the pseudoforce method differs among various computer programs. In MSC/NASTRAN, the nonlinear forces are evaluated at the end of one time step for use in the successive time step. The equations of motion became

$$[M]\{\ddot{x}(t)\} + [C]\{\dot{x}(t)\} + [K]\{x(t)\} = \{f(t)\} + \{n(t-\Delta t)\} \qquad (2)$$

Note that the nonlinear force lags the true solution by a time step, which may require use of small integration time steps (smaller than those required for a purely linear analysis). This is discussed in the appendix.

Equation 2 can be solved in modal or physical coordinates. For all examples discussed in this paper, direct integration was chosen to avoid the question of mode truncation that arises in mode superposition; points made here, however, should apply equally to mode superposition.

The NOLIN1 dynamic load is used to represent the nonlinear force. It is used in conjunction with a linear elastic element to produce the desired force-deflection curve, which is illustrated in Figure 2. The NOLIN1 dynamic force is formulated on a TABLED1 card, which contains a force-versus-deflection table describing the nonlinear force. For desired force-deflection curves more complicated than the bilinear stiffness shown in the figure, the nonlinear force is made correspondingly more complex.

The appendix presents validation of the pseudoforce method for simple problems, and also illustrates effects of the integration time step on solution accuracy. Recent use of the pseudoforce method on large problems is described in the following sections.

THRUST TURBINE EXAMPLE

A finite element model of two thrust turbines, their common subbase, and the subbase rubber shock isolators was formulated using MSC/NASTRAN. This system is part of the propulsion system of the three-thousand-ton Surface Effect Ship (3KSES) that was to be built by RMI (formerly Rohr Marine, Inc.) for the Navy. The objective of the analyses was to perform structureborne noise decoupling calculations [3] and to perform loads and motion analysis of the thrust turbines/subbase/subbase support system [4]. The latter analysis is described herein.

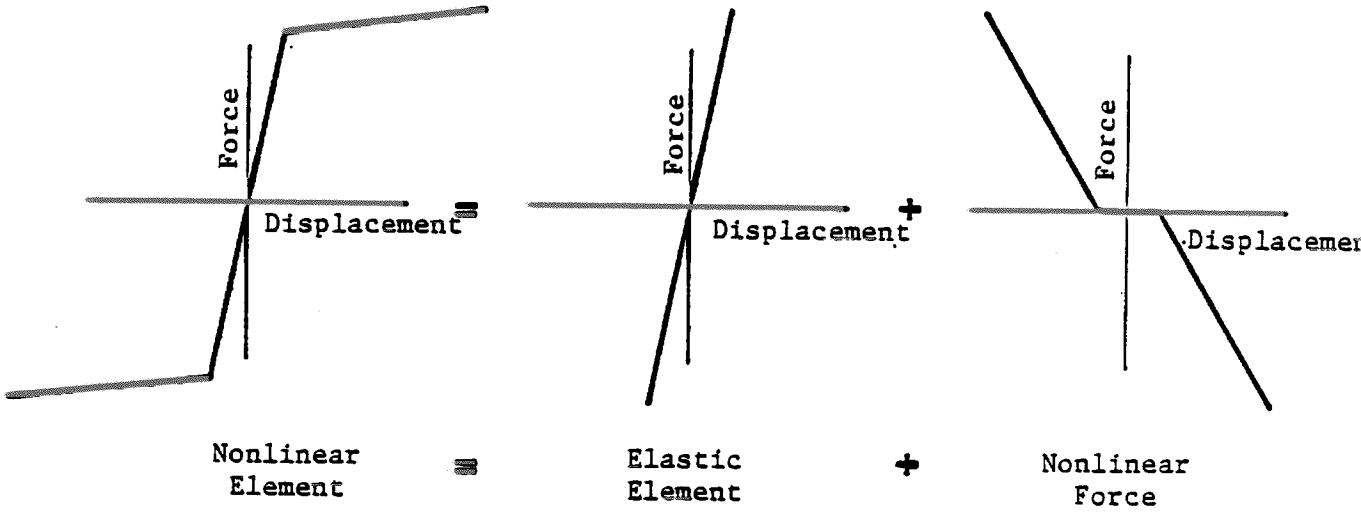

Figure 2: Formulation of Nonlinear Element

A drawing of one of the turbines mounted on its subbase is shown in Figure 3. The subbase is mounted on 46 vertical rubber shock isolators that possess nonlinear elastic force-deflection characteristics. A flexible turbine shaft coupling, located at the aft end of each shaft, was analyzed to assess its loads and deformation under wave loading of the ship.

Each turbine was modeled with equivalent beam, spring, and mass properties, and contained 66 DOF. The subbase, containing 432 DOF, was modeled with beam elements. The rubber mounts are each hardening systems with force-deflection characteristics as shown in Figure 4. Each mount is modeled with a linear spring and a nonlinear force in a manner similar to that shown in Figure 2. Two constraints were imposed on selection of mount stiffnesses: (1) the system (turbines plus subbase) must remain level under gravity loading; and (2) the first vertical frequency, with the system remaining level, must be either 5 Hz or 7 Hz, depending upon which case is analyzed. These constraints give factors that define linear spring stiffnesses for the subbase regions (see Figure 5) and that define values of the nonlinear forces. Transfer functions and extra points were used to define relative displacement between the subbase and hull to determine the nonlinear force to be applied to the subbase.

Vertical transient motion, which consisted of a decaying exponential plus a decaying sinusoid, was enforced on the ship's hull. One second of this motion was analyzed using direct integration with an integration time step of 0.005 s. Loads in the rubber mounts and relative displacements and rotations in the flexible shaft coupling were computed. Maximum loads and relative motions were lower for the stiffer (7 Hz) mounts than for the softer (5 Hz) mounts.

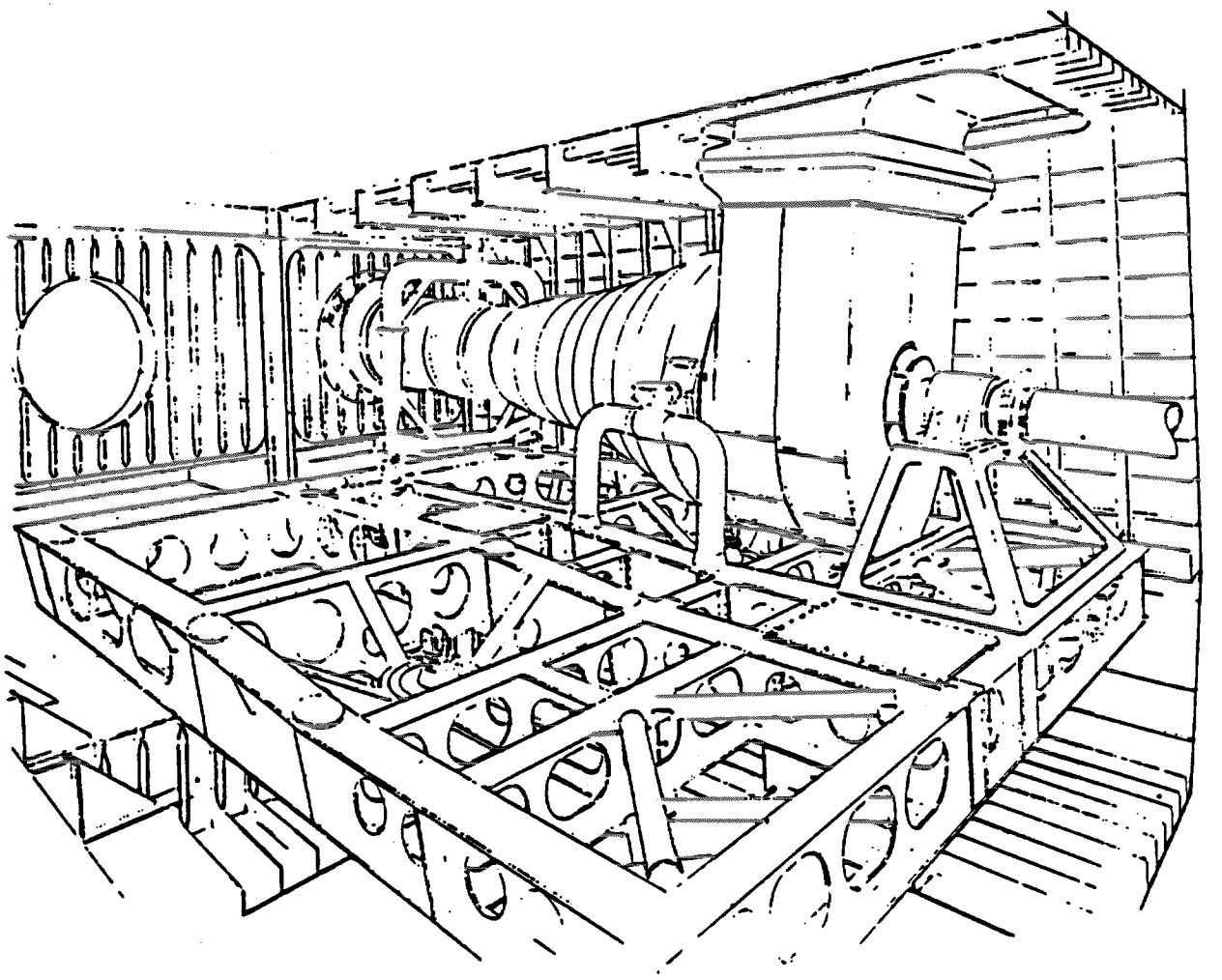

Figure 3: Turbine/Subbase Layout

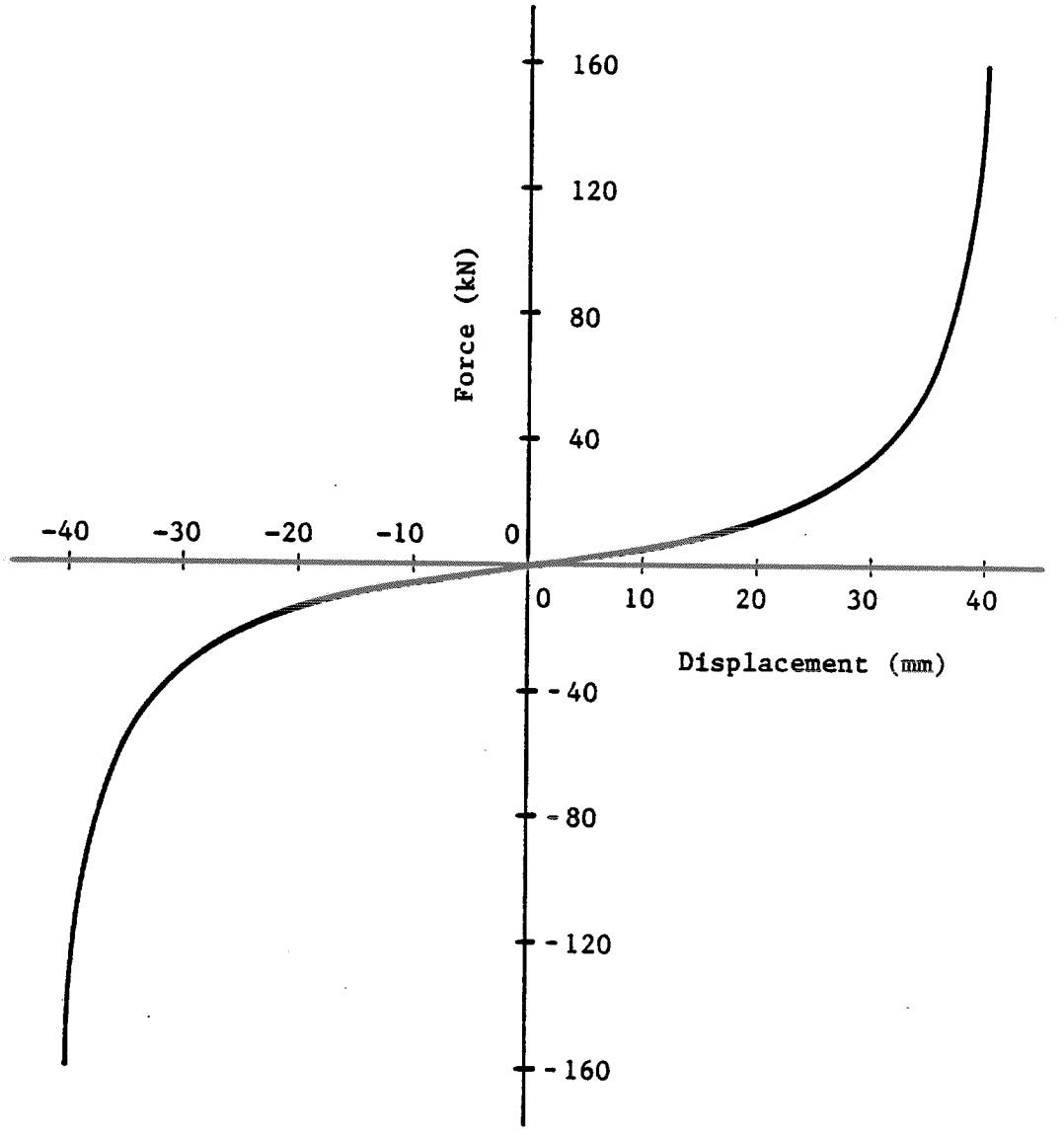

Figure 4: Force-Versus-Displacment Curve for Rubber Shock Isolator

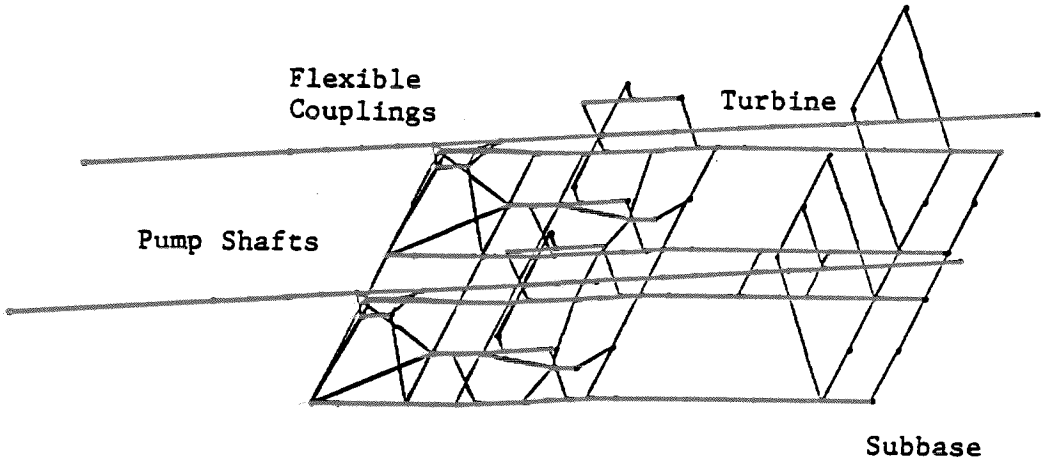

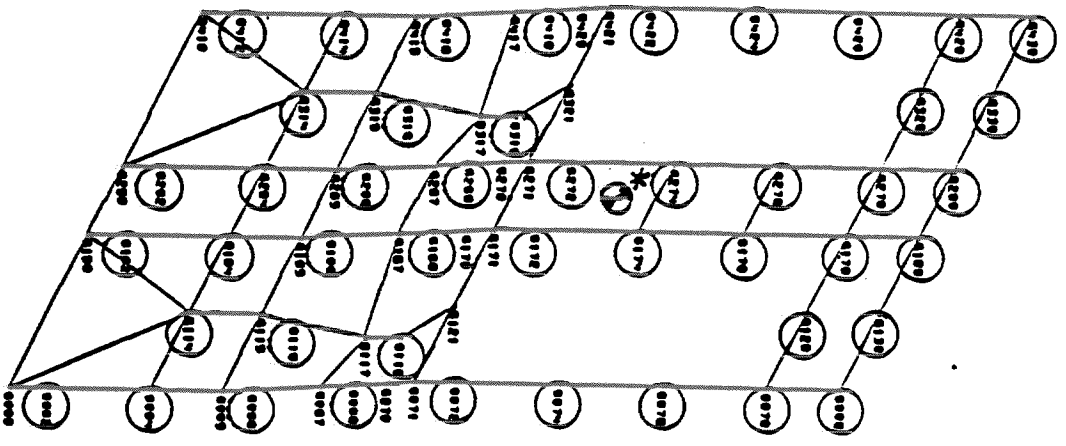

*Center of gravity of the subbase/turbines system

Figure 5: Finite Element Schematic (Top) and Rubber Mount Locations (Bottom)

PIPING SYSTEM EXAMPLE

The containment structure and several piping systems of the decommissioned Heissdampfreaktor nuclear power plant (near Kahl, West Germany) were dynamically tested to provide a data base against which to benchmark analytical models and modeling techniques. Extensive snapback and sine-dwell tests were performed on the nonlinear recirculation loop (URL), a schematic of which is shown in Figure 6. Snapback tests were performed [5] by: (1) applying a preload at Node 101 (see the figure); (2) allowing the dynamic transients to decay; (3) quickly releasing the preload; and (4) monitoring resulting free-vibration piping response. Twenty-four acceleration time histories were measured for each test. Four snapback tests were performed, with different preloads and forcing directions. Two such tests were simulated analytically [6,7]; these were the 80-kN and 220-kN snaps in the X' direction.

The URL piping system consists of water-filled piping, the reactor pressure vessel, and two large recirculation pumps. The pipe and reactor pressure vessel are grounded by fixed points. In addition, the pipe is supported by four spring hangers, twelve constant force hangers, and twelve nonlinear swaybraces; pipe support locations and idealized behavior are shown in Figures 7 and 8, respectively.

A 774 dynamic DOF finite element model was formulated using MSC/NASTRAN. All pipe materials were modeled to be linear elastic; the spring hangers were modeled as linear springs, and the constant force hangers were neglected in the simulation (due to their exertion of a constant force for displacements within their working range). Swaybrace static force-deflection data were obtained [8] prior to snapback testing, and are plotted in Figure 9. Idealized swaybrace behavior for use in the model is shown in Figure 10; note that the slight measured hysteresis was ignored in the model, allowing each swaybrace to be modeled as nonlinear elastic. A linear spring (with stiffness k_1) and a NOLIN1 dynamic load were used to represent each swaybrace in the manner depicted in Figure 2.

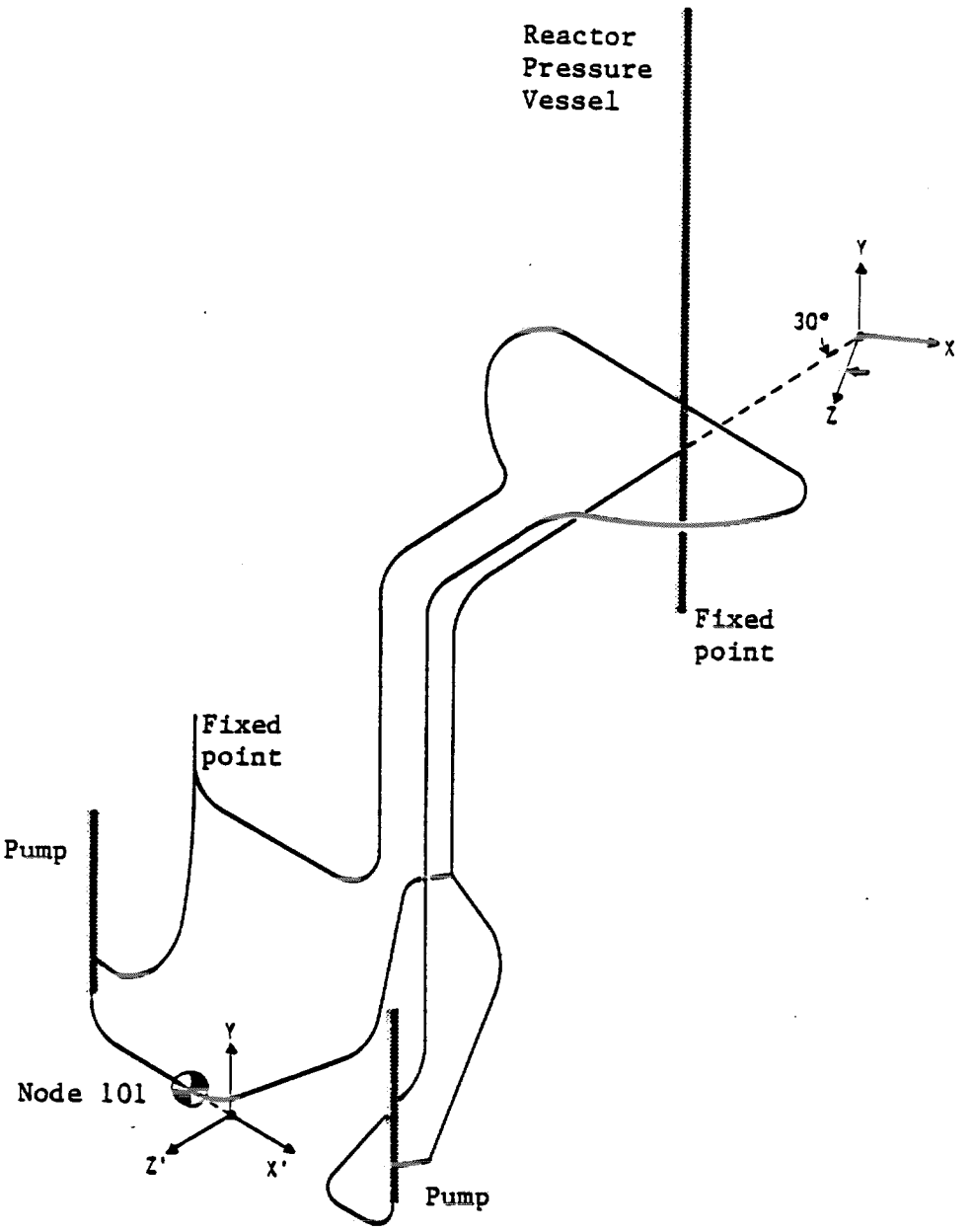

Figure 6: Schematic of URL Piping System

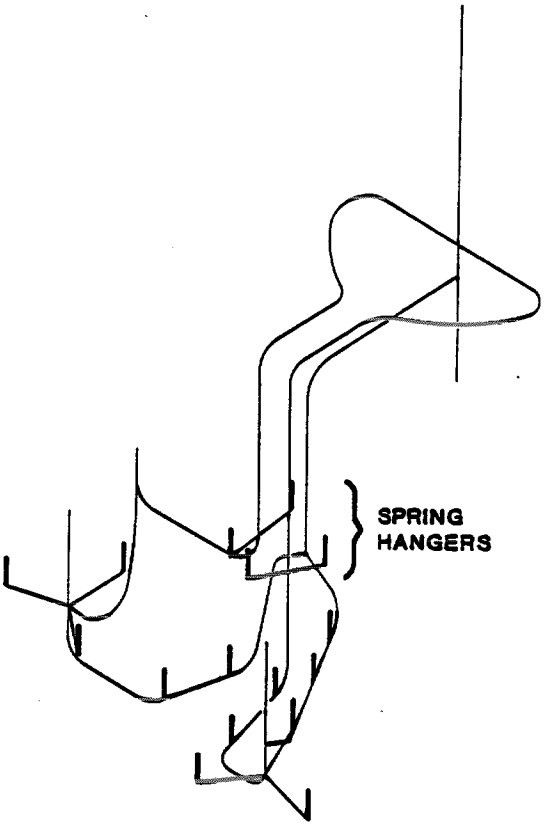

SPRING AND CONSTANT FORCE HANGER LOCATIONS

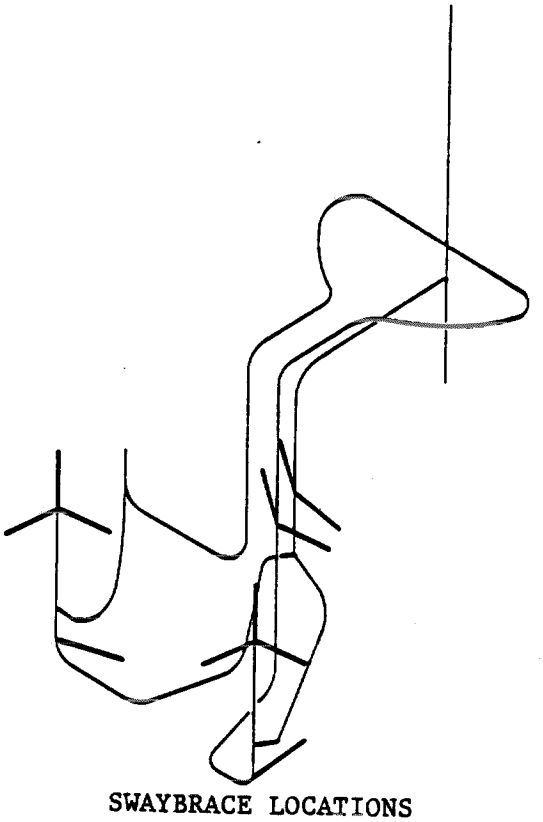

SWAYBRACE LOCATIONS

Figure 7: URL Hanger Locations

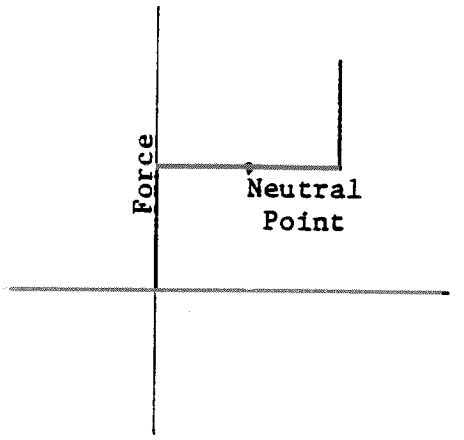

IDEAL BEHAVIOR FOR CONSTANT FORCE HANGERS

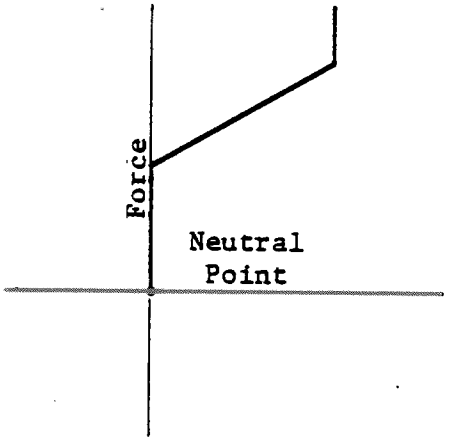

IDEAL BEHAVIOR FOR SWAYBRACES

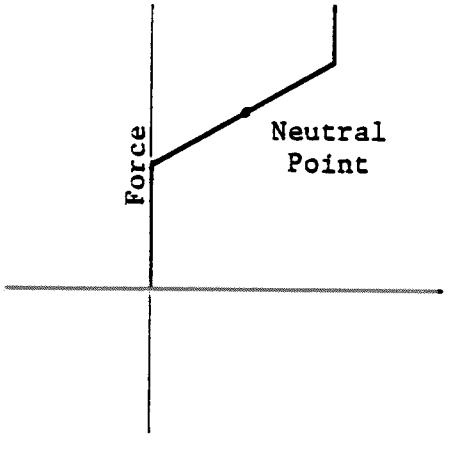

IDEAL BEHAVIOR FOR SPRING HANGERS

Figure 8: Ideal Behavior for URL Hangers

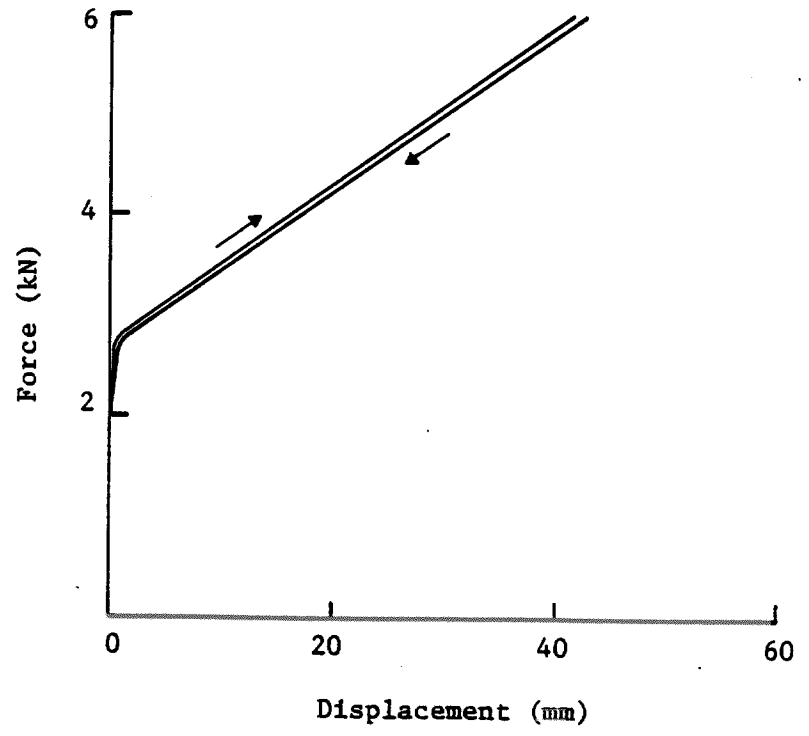

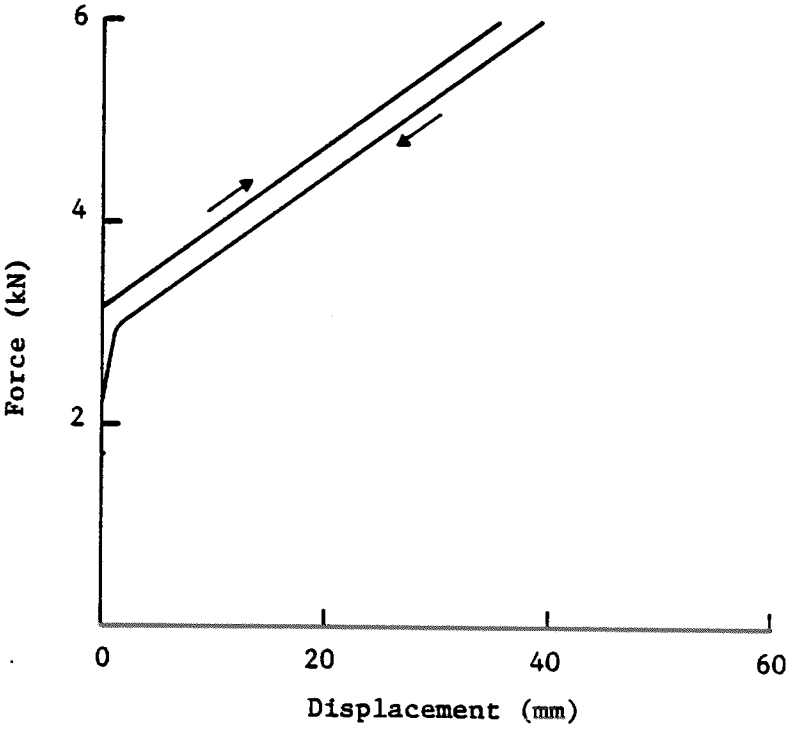

Figure 9: Measured Behavior for Swaybraces

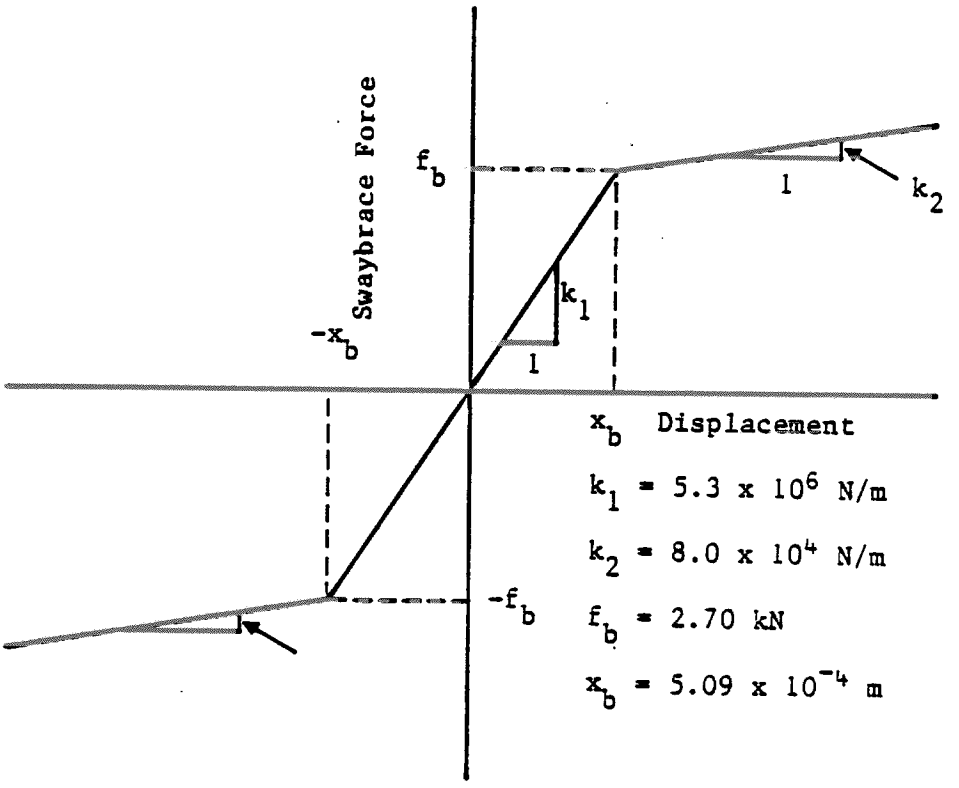

Figure 10: Idealized Swaybrace Behavior

Prior to simulating the snapback tests, the pseudoforce method was validated on a single swaybrace to validate the pseudoforce method and to ensure correct swaybrace representation. Also, proper incorporation of every nonlinear swaybrace into the model was checked using an efficient piecewise linear analysis algorithm. These are detailed in the appendix.

Since the pseudoforce method is available only for transient analyses, the preload was simulated by applying a step load and allowing the dynamic transients to decay. Then, the load was quickly decreased to zero, resulting in subsequent free-vibration response that was simulated for 2.5 s (using an integration step size of 0.005 s). Multipoint constraints (MPCs) were utilized to output nodal accelerations that corresponded to measurement directions. These analytical accelerations were written to the PUNCH file for subsequent postprocessing (plotting and Fourier transforming) in the same manner as were the test measurements.

Two models were formulated: one was the nonlinear model that represented each swaybrace with NOLIN1 dynamic loads, and the other was a linear model that represented each swaybrace with an average, equivalent stiffness (between k_1 and k_2--see Figure 10). Typical data/nonlinear model/linear model time and frequency domain comparisons are shown in Figure 11. Peak acceleration (positive and negative) response comparisons are shown in Figure 12. The linear and nonlinear models closely matched the test data for the 80-kN snap, whereas the nonlinear model was much better than the linear model for the 220-kN snap. Comparison of other responses--general form and frequency content of the acceleration time histories and swaybrace force time histories--showed the nonlinear model to be substantially superior to the linear model for both snapback simulations.

High-level seismic excitation was also simulated. Transfer functions and extra points were required (see the appendix) to represent relative motion of the swaybrace ends. The nonlinear model was compared to a linear

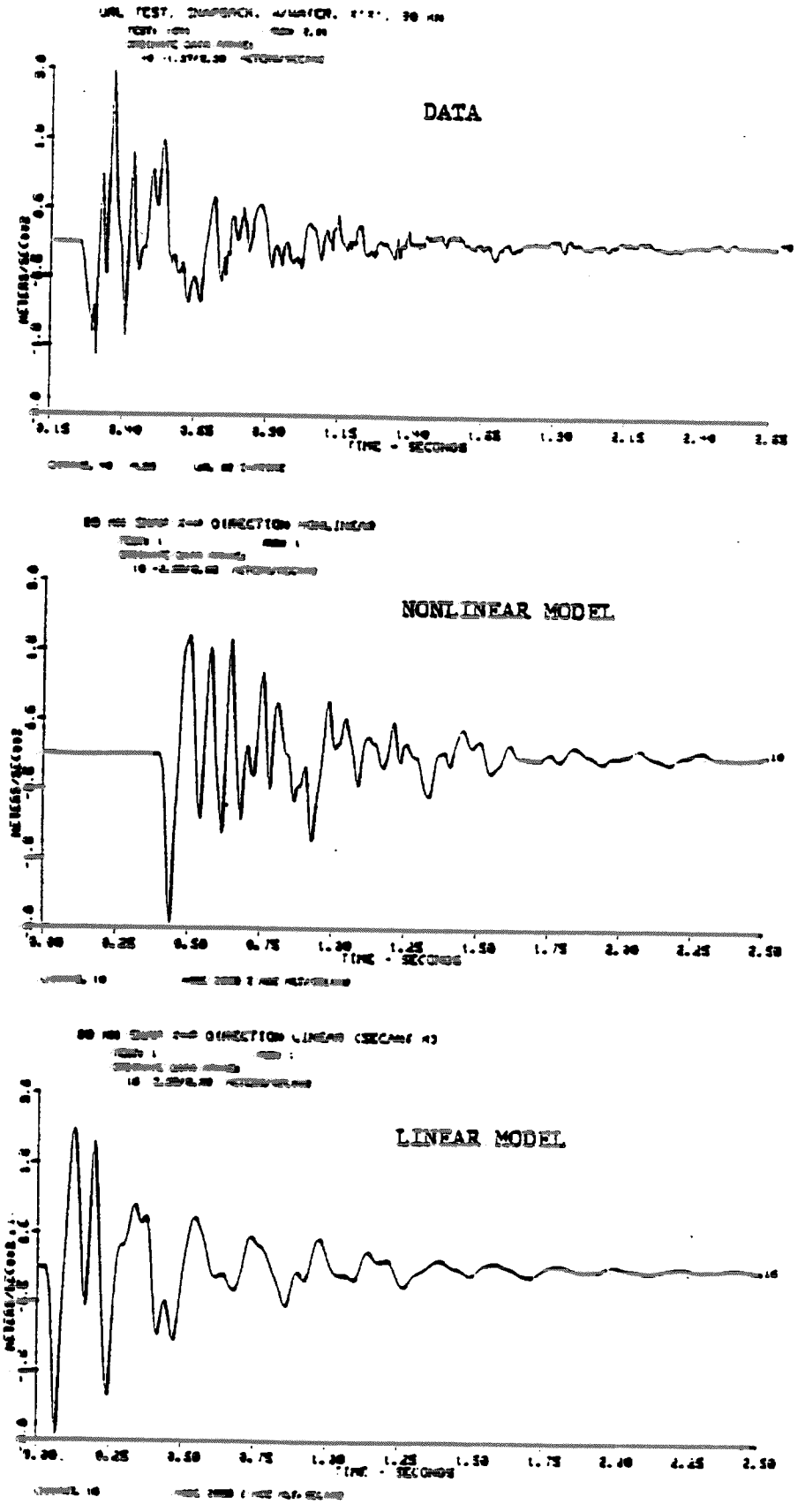

Figure 11: Typical Acceleration Comparisons--Time and Frequency Domains

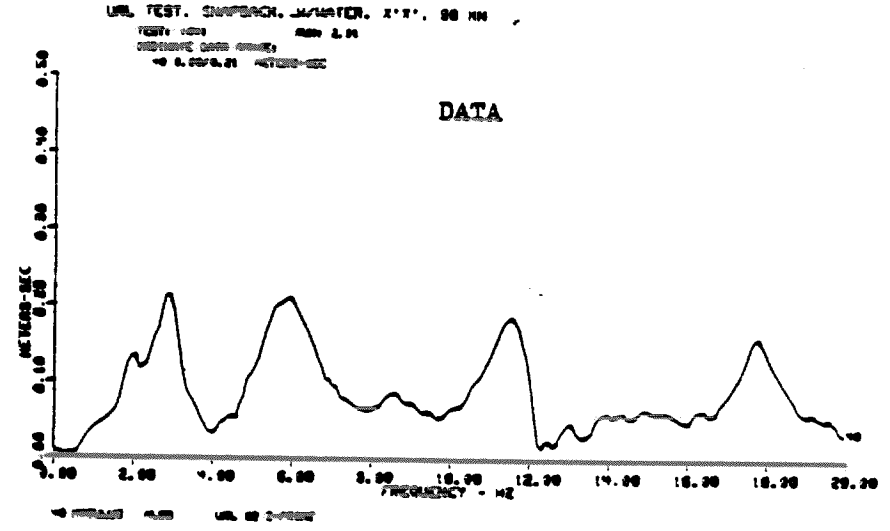

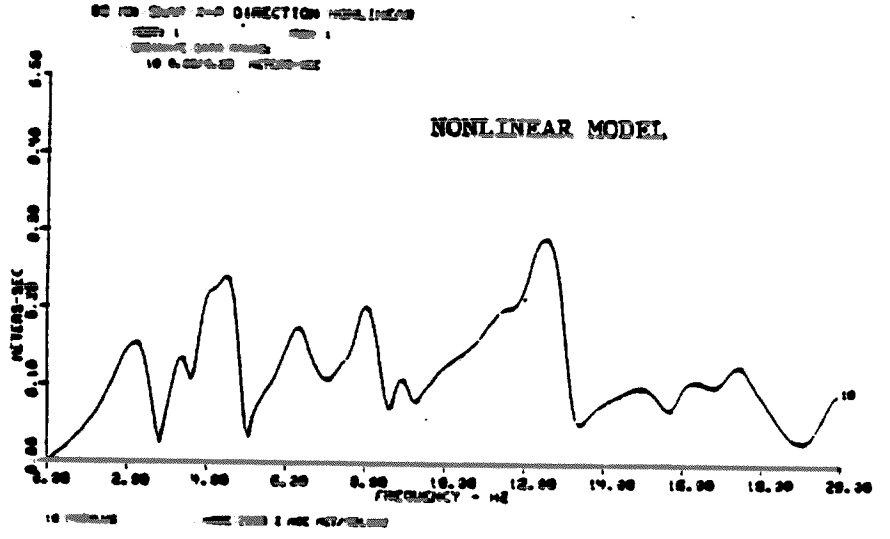

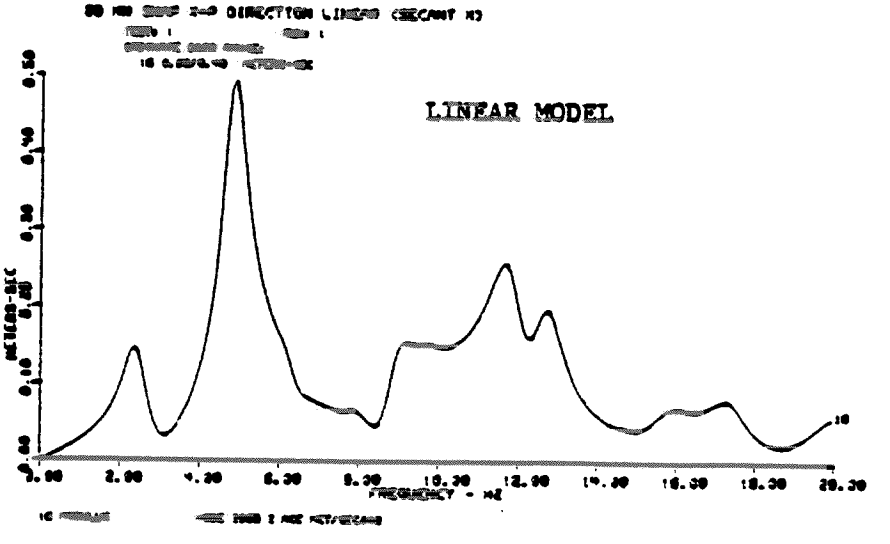

Figure 11 (Continued)

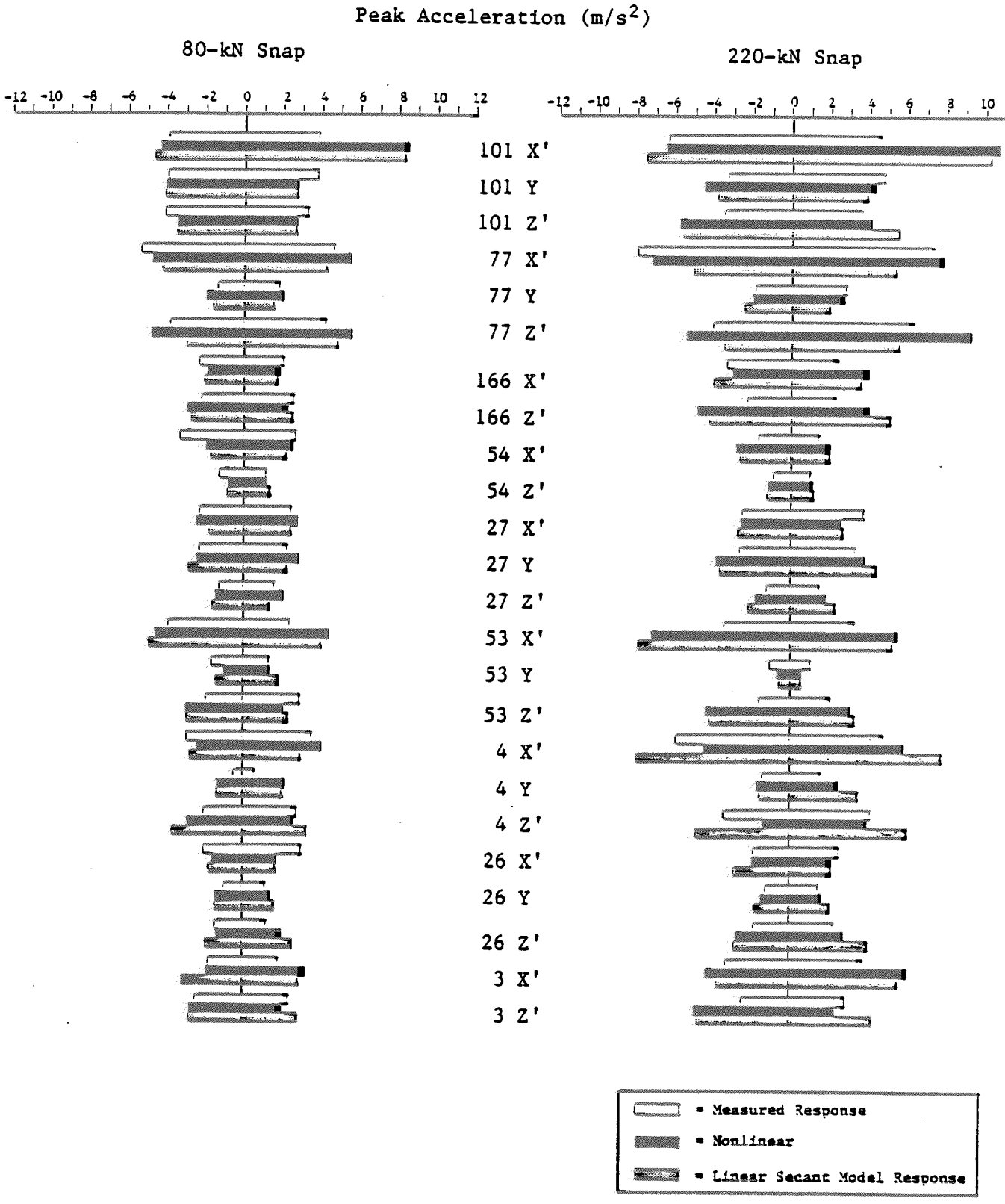

Figure 12: Peak Acceleration Response Comparisons

model that represented all swaybraces as linear springs with stiffness k_1. Element stresses were considerably lower (by 25-75%) for the nonlinear model.

CONCLUSIONS

The two examples illustrated recent usage of the pseudoforce method in MSC/NASTRAN for efficiently modeling nonlinear elastic systems. Direct integration was used to solve the equations of motion, though mode superposition could have been used as well. The technique was efficient in that it required no more computer time than did a comparable, purely linear analysis. The technique was accurate in that the computed force-deflection curves matched the desired curves to a reasonable degree (see the appendix).

As shown in the URL piping example, accurate representation of system nonlinearities better matches reality than does an equivalent linear model; it is again emphasized that a more accurate model resulted without incurring a computational penalty. Additionally, the lower element stresses resulting from the nonlinear model indicate the potential usefulness of the pseudoforce method in piping design.

ACKNOWLEDGEMENTS

The authors are appreciative of RMI and the Nuclear Regulatory Commission for sponsoring the 3KSES and HDR URL simulations, respectively.

We would also like to thank our colleagues, Dan Chitty, George Howard, Blake Johnson, Chris Kato, Cheryl Minor, Terry Scharton, and Frankie Spalding for their assistance in those projects and in the preparation of this paper.

REFERENCES

1. R. H. MacNeal, editor, The NASTRAN Theoretical Manual, The MacNeal-Schwendler Corporation, Los Angeles, CA, December 1972.

2. J. A Joseph, MSC/NASTRAN Application Manual, The MacNeal-Schwendler Corporation, Los Angeles, CA, April 1982.

3. "Structureborne Noise Decoupling on 3KSES Propulsion Gas Turbine," ANCO Engineers, Inc., Report No. 1291.1, September 1978.

4. "Loads and Motion Analysis of Thrust Turbines/Subbase/Subbase Supports for the 3KSES," ANCO Engineers, Inc., Report No. 1291.1, October 1978.

5. "Intermediate and High-Level Forced Vibration Tests at the Heissdampfreaktor (HDR)," ANCO Engineers, Inc., Report 1083.10R, June 1980.

6. K. D. Blakely, et.al., "Pipe Damping Studies and Nonlinear Pipe Benchmark from Snapback Tests at the Heissdampfreaktor," NUREG/CR-3180, March 1983.

7. K. D. Blakely, et.al., "Comparison of a Nonlinear Dynamic Model of a Piping System to Test Data," Paper F 5/4, to be presented at the 7th SMiRT Conference, Chicago, Illinois, August 1983.

8. "Experimentelle Ermittlung der Kennlinien von Rohrleitungshängern am Rohrleitungssystem im HDR-Kahl," Battelle-Institute, Frankfurt, November 1978.

APPENDIX: VALIDATION OF THE PSEUDOFORCE METHOD

Four validations of the pseudoforce method were performed. Static and dynamic validations were done, each with a simple and a complex (the 774 DOF piping system) model.

Static Solution Benchmark--Simple Model

A simple model was chosen to assess accuracy of the pseudoforce method for nonlinear static problems. The model, shown in Figure A.1, consisted of a cantilever beam with a nonlinear elastic spring attached to the tip. Also shown in the figure are the nonlinear force-deflection characteristics.

The pseudoforce method, as implemented in MSC/NASTRAN, is available only for dynamic transient analyses. In order to circumvent this restriction for the static benchmark, the force is applied as a step load, and the static solution is obtained after the dynamic transients have decayed to negligilbe levels.

The effective stiffness at the tip, k_t, is given by

$$k_t = k_s + k_c \tag{A.1}$$

where k_s denotes the spring stiffness, and k_c denotes the cantilever stiffness which is given by

$$k_c = \frac{3EI}{L^3} = \frac{(3)\ (1000)\ (0.5)}{(2)^3} = 187.5 \text{ lb/in.} \tag{A.2}$$

The spring stiffness is given by

$$k_s = \begin{cases} k_1 = 2000 \text{ lb/in. for } |\Delta| \leq 0.333 \text{ in.} \\ k_2 = 66 \text{ lb/in. for } |\Delta| \leq 0.333 \text{ in.} \end{cases}$$

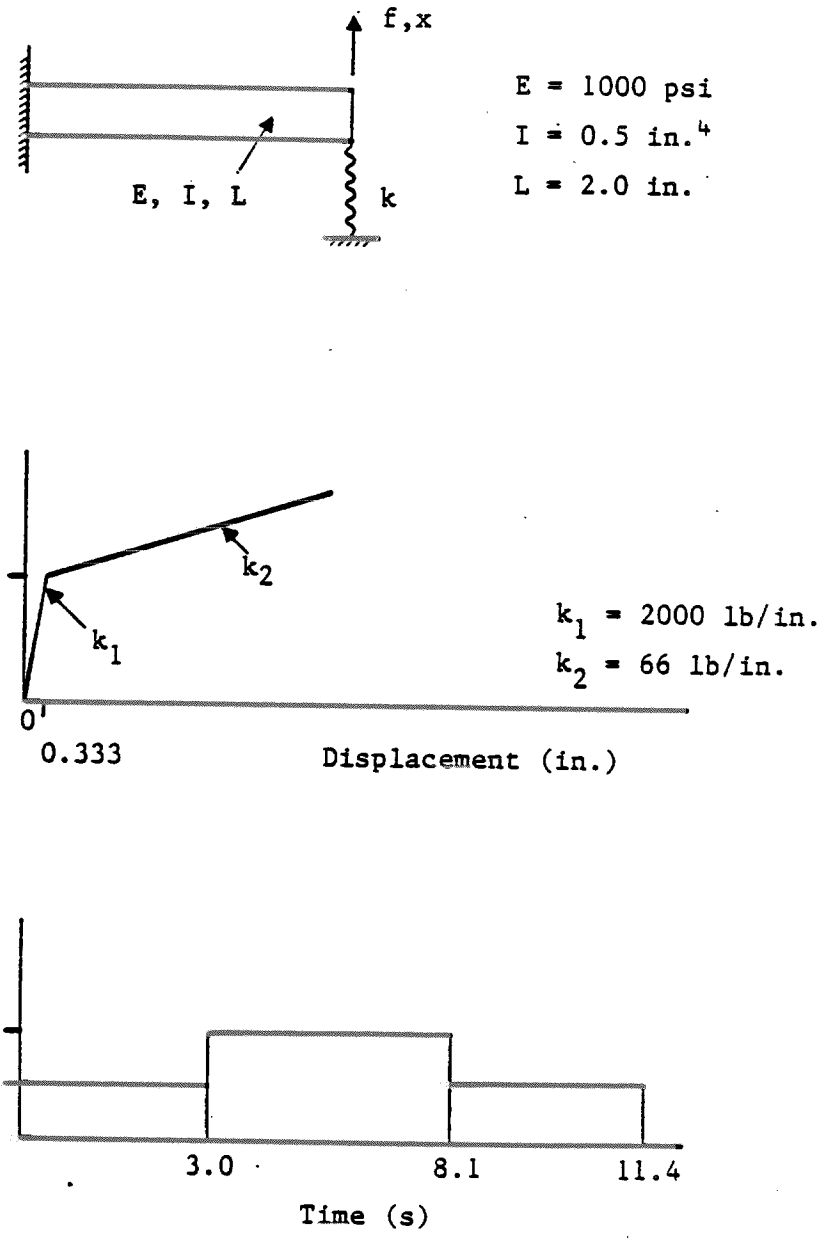

Figure A.1: Model and Loading for Static Solution Benchmark

A load of 500 lb was applied to the cantilever tip; MSC/NASTRAN gave a tip displacement of 0.2280 in. (once the dynamic transients had sufficiently decayed). Note that this displacement is less than 0.333 in., and the spring remains in the k_1 region. Therefore, the exact static displacement is given by

$$\Delta = \frac{f}{k_t} = \frac{f}{k_s + k_c} = \frac{500}{(2000 + 187.5)} = 0.2286 \text{ in.} \qquad \text{(A.3)}$$

to which the MSC/NASTRAN-computed result compares favorably.

The tip load was then increased by 500 lb (to 1000 lb); MSC/NASTRAN gave a tip displacement of 1.39 in. (after the transients decayed). Note that this displacement is greater than 0.333 in. and that the spring should be in the k_2 region. Therefore, the exact static displacement is given by

$$f_n = f - f_b \quad (f = 1000 \text{ lb})$$
$$f_b = (k_s + k_c)\,(\Delta_b) = (2000 + 187.5)\,(0.333) = 728.44 \text{ lb}$$
$$\Delta = \Delta_b + \frac{f_n}{k_s + k_c} = 0.333 + \frac{271.56}{(66 + 187.5)} = 1.40 \text{ in.} \qquad \text{(A.4)}$$

to which the MSC/NASTRAN-computed result compares favorably.

The tip load was then decreased to 500 lb to verify solution accuracy upon unloading; MSC/NASTRAN gave a tip displacement of 0.2292 in., which compares favorably to the exact static displacement of 0.2286 in.

Thus, the pseudoforce method in conjunction with direct integration was validated for the static response of a simple nonlinear elastic structural system.

Dynamic Solution Benchmark--Simple Model

A simple model was chosen to assess accuracy of the pseudoforce method for nonlinear dynamic problems. The model, shown in Figure A.2, consisted of two truss elements, a single concentrated mass, and two springs (one of which

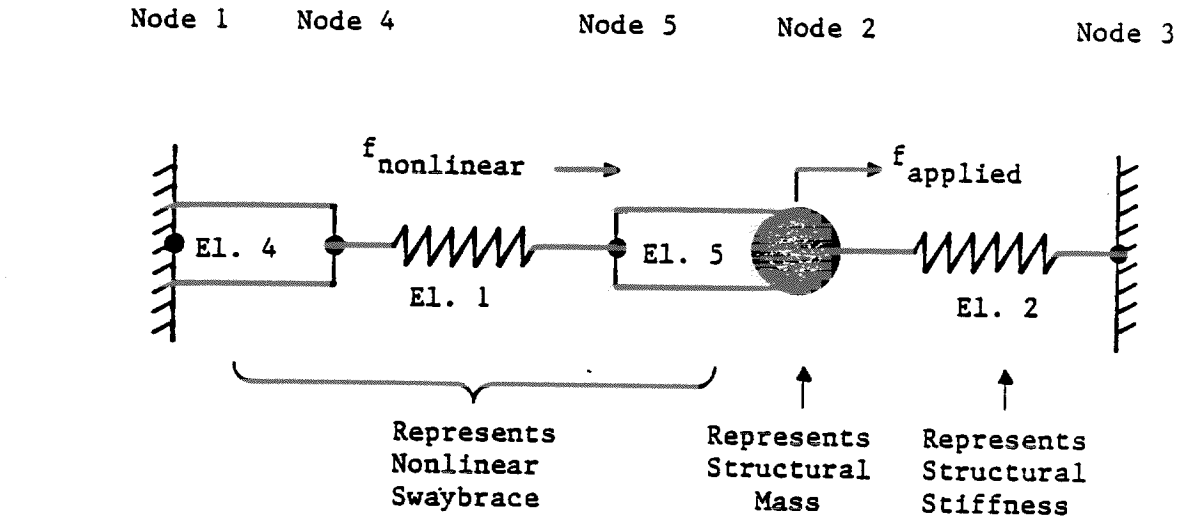

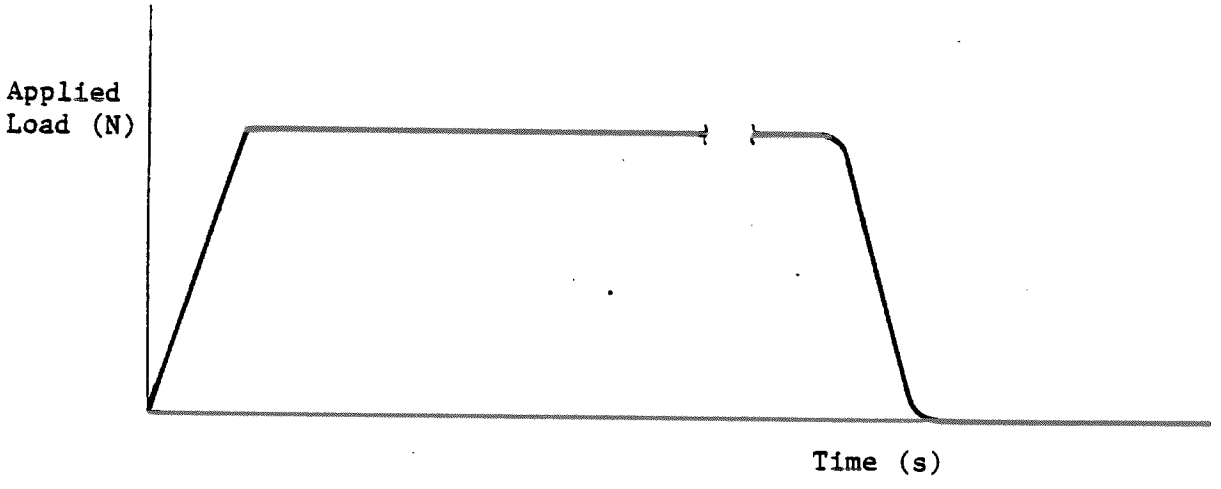

Figure A.2: Model and Loading Dynamic Solution Benchmark

was nonlinear). The mass and stiffnesses were selected such that when both springs are in the k_1 region (see Figure A.1), the system resonant frequency is 2.8 Hz; when the nonlinear spring is in the softer k_2 region, the system resonant frequency is 2.0 Hz.

The remainder of the model was chosen to represent each swaybrace as simulated in the piping system model. In MSC/NASTRAN, the nonlinear forces are most easily applied in a local coordinate system, which is defined by Nodes 4 and 5. The two trusses, therefore, connect the local coordinate system nodes to global coordinate system nodes (represented by Nodes 1 and 2 in the simple model). Each truss is massless, short, and stiff though it is not too stiff to cause ill-conditioning of the system stiffness matrix. The first truss grounds Node 4, and the second truss yields the swaybrace force (linear spring force plus nonlinear force).

Snapback tests (see text) were simulated with the simple system. Figure A.2 shows the applied loading time history; dynamic transients had sifficiently decayed prior to simulating release of the static preload. Figure A.3 shows response time histories for the displacement and acceleration at Node 5 and for the force in Element 5 (equivalent to the swaybrace force). Dynamic response was calculated using the Newmark-β method, with an integration time step of 0.017857 s (giving 20 points per cycle for 2.8-Hz response).

This benchmark illustrates the nature of the pseudoforce method. In reality, this example is one of free-vibration response after release of the preload, with the system stiffness changing with time. However, in the pseudoforce method this example becomes one of forced response of a linear system, with the loading being applied via the nonlinear force. This loading is such that at high levels of response the 2.8-Hz system vibrates at 2.0 Hz; thus, the nature of the problem has been changed from free response to forced response.

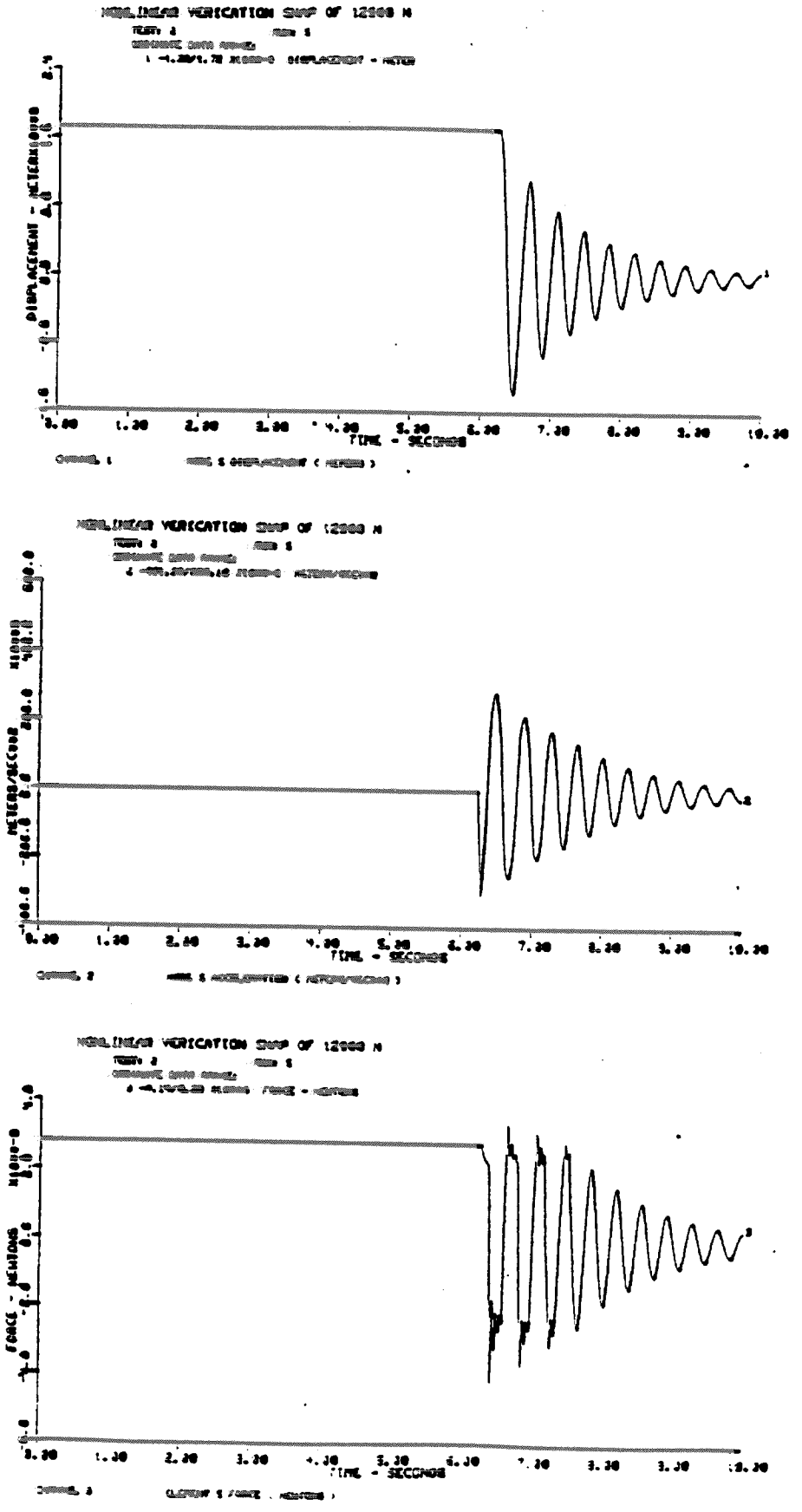

Figure A.3: Response Time Histories for the Nonlinear SDOF System

A check was made to assess accuracy of the pseudoforce method for this simple snapback example. The swaybrace force-versus-displacement curve was plotted for this example and is shown in Figure A.4a; the desired swaybrace force-deflection curve is shown in Figure A.4b, superimposed over the computed curve. Deviation from the desired curve is apparent, in particular for forces and displacements outside of the desired k_1 range. This deviation results because the true nonlinear force lags the computed response by a time step. Another simple snapback example problem was run, this one with an integration time step of 0.035714 s (double that of the previous example). Figure A.5 shows the computed force-deflection curve. As expected, deviation from the desired characteristics is much more pronounced when using the larger Δt. Thus, the integration time step is a significant factor--even more so than in a purely linear analysis--in obtaining an accurate solution via the pseudoforce method.

Static Solution Benchmark--Complex Model

As a check on proper incorporation of the twelve swaybraces into the piping system model, static analyses (obtained by applying a step load and allowing the dynamic transients to decay) of the nonlinear model using the pseudoforce method were compared to nonlinear analysis results obtained using static structural reanalysis algorithms. This was done for both the 80-kN and 220-kN X' snapback loads which were applied to the piping system.

Structural reanalysis involves resolving a system of equations for a structure that has been locally modified. The reanalysis procedure solves a problem of much lower order than the original problem and, hence, is computationally much more efficient for locally modified structures than is complete reformulation and redecomposition. In essence, the structural reanalysis problem is stated as follows

$$\begin{aligned} &\text{given } [K]\ \{x\} = \{f\},\ [K] = [L][D][L]^T, \text{ and } [\Delta K] \\ &\text{solve } [K+\Delta K]\ \{x+\Delta x\} = \{f\} \end{aligned} \tag{A.5}$$

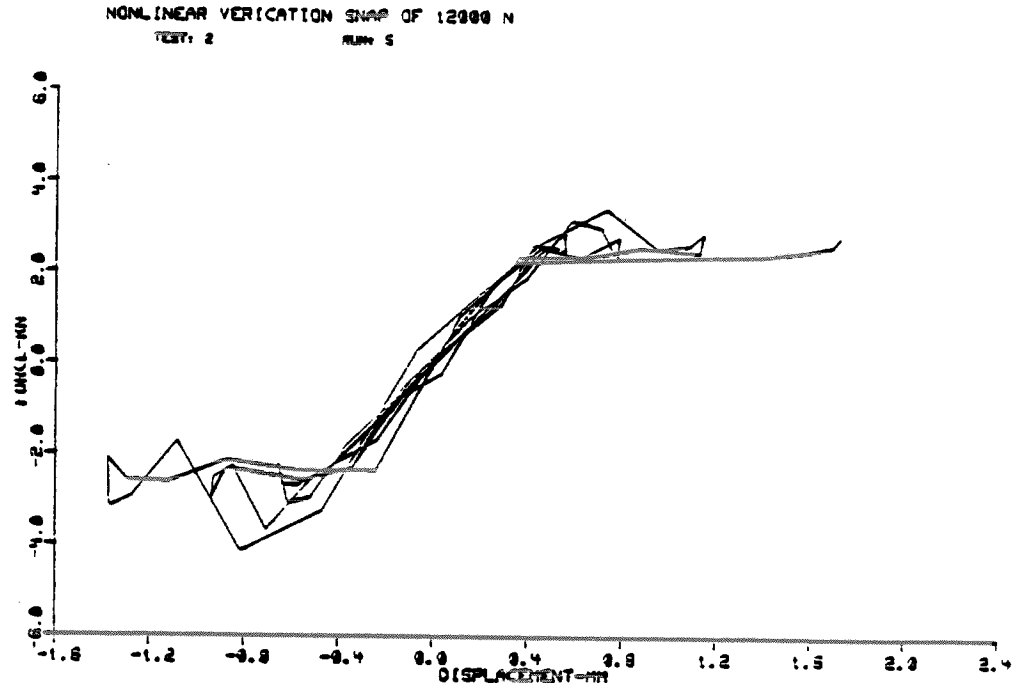

a. Computed Force-Deflection Curve

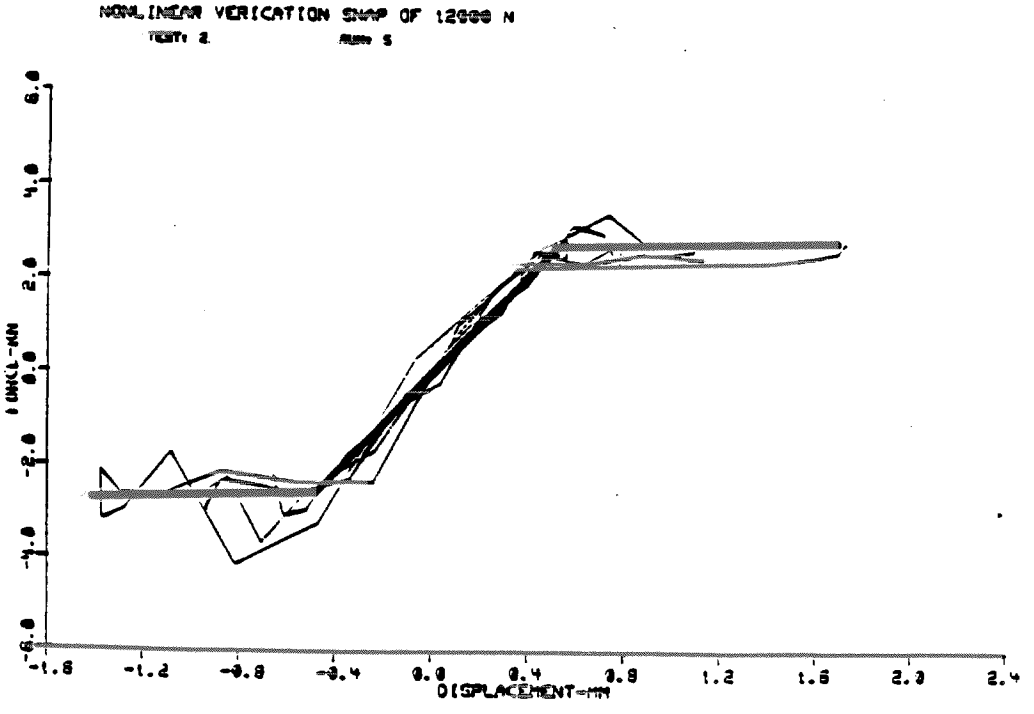

b. Comparison to Ideal Curve

Figure A.4: Computed Force-Deflection Curve and Comparison to Ideal Curve

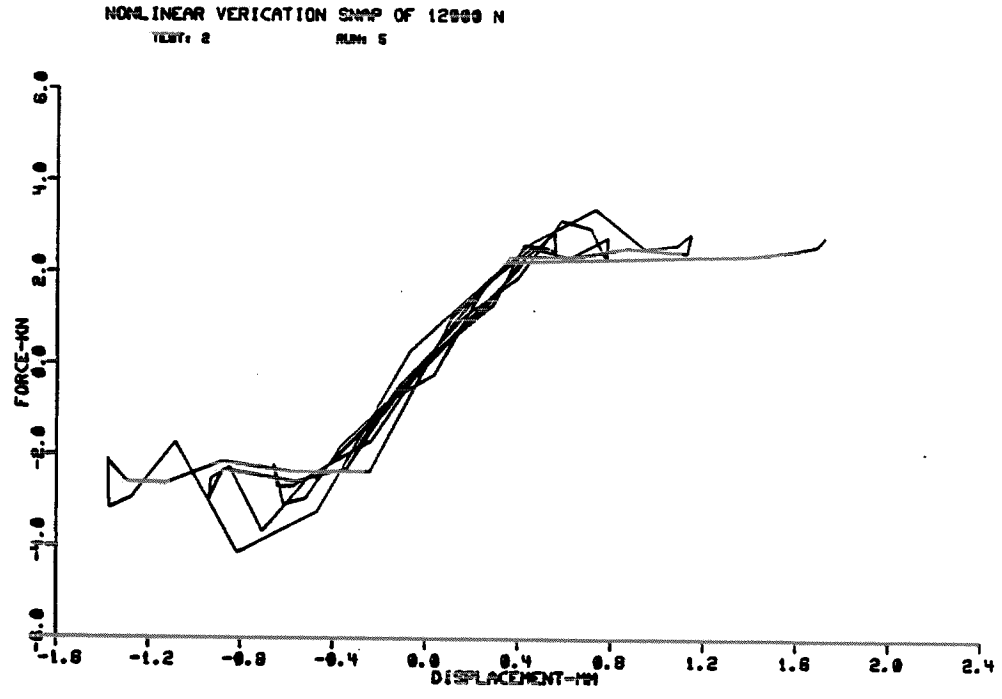

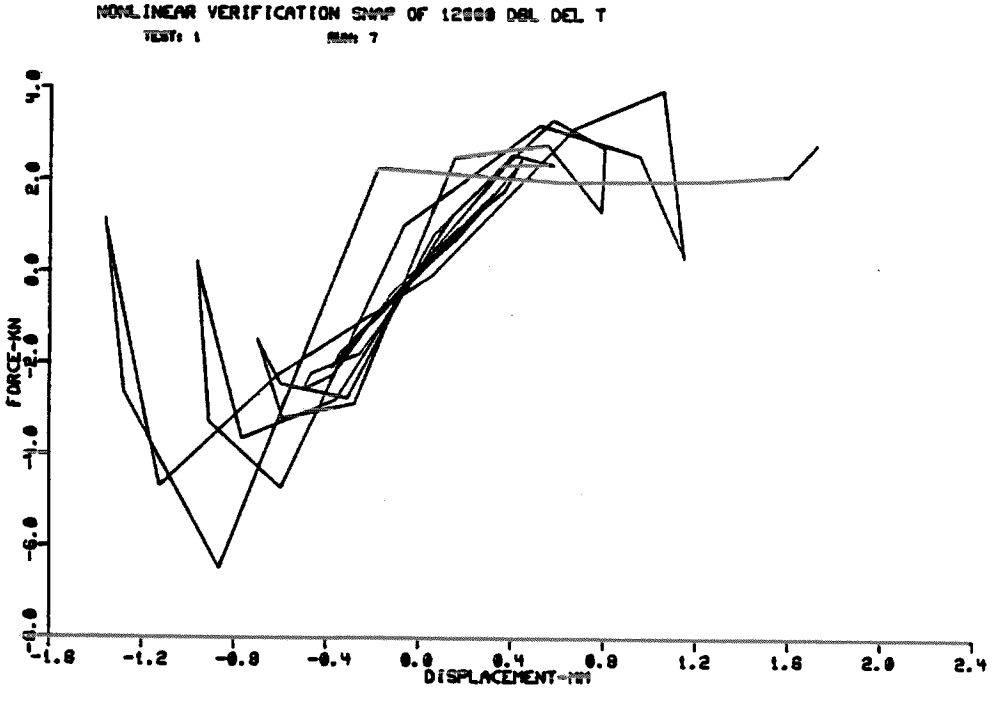

Figure A.5: Effect of Integration Time Step on Computed Force-Deflection Curve--SDOF System

Note that [ΔK], the modification to the system stiffness matrix, cannot be such that the sum [K+ΔK] becomes a singular matrix. Also, whereas [ΔK] may contain relatively few (when compared to [K]) nonzero entries, each entry may have a large magnitude; hence, the corresponding changes to the solution vector, {Δx}, may also be large.

Many efficient algorithms have been proposed to solve Eq. A.5 (see Refs. A.1 and A.2 for a comprehensive review of the different structural reanalysis techniques). For the piping system project, the Sherman-Morrison algorithm [A.3]* was used, which--for the type of structural modifications analyzed in the piping system--reduced to the pseudoforce method for structural reanalysis [A.4].

The Sherman-Morrison identity, stated here without proof, is

$$[K + BCD]^{-1} = [K]^{-1} - [K]^{-1}\,[B]\,[C^{-1} + DK^{-1}B]^{-1}\,\,[D]\,[K]^{-1} \qquad (A.6)$$

where [K] is the original matrix (of dimension n x n), and the product [BCD] represents the modified matrix (or, [ΔK]). Note that [C] cannot be singular, nor can $[C^{-1} + DK^{-1}B]$.

For structural reanalysis, [K] is the system stiffness matrix, and [BCD] is the modified stiffness matrix; both [K] and [BCD] are in global coordinates. To make the algorithm efficient, the size of [C]--and, hence, $[C^{-1} + DK^{-1}B]$--should be as small as possible. To accomplish this, [C] should be of dimension m x m, where m represents the number of locally modified degrees-of-freedom (and, as such, m<<n). Then, since [ΔK] is symmetric for structural analysis, [B] and [D] are the transposes of each other. If [C] is in global coordinates, [B] and [D] are Boolean matrices (ones and zeroes) that properly expand [ΔK] from size m x m to size n x n. If [C] is in local coordinates, a rotation matrix is also incorporated into [B] and [D]. For the piping system, the size of [C] is 12 x 12 (as compared to the size of [K], which is 774 x 774); [C] is a diagonal matrix representing (at most) 12 stiffness changes. The matrices [B] and [D], therefore, are simply Boolean matrices, since [C] is in global coordinates.

*Numbers in brackets denote references.

As shown in Eq. A.6, the global stiffness matrix inverse can be modified. However, since the original inverse was never explicitly computed, only the updated solution vector was sought. This is accomplished by post-multiplying Eq. A.6 by the applied load vector, {f}, as follows

$$[K + BCD]^{-1}\{f\} = [K]^{-1}\{f\} - [K]^{-1}[B][C^{-1} + DK^{-1}B]^{-1}[D][K]^{-1}\{f\} \quad (A.7)$$

or, since $[K]\{x\} = \{f\}$

$$\{x + \Delta x\} = \{x\} - [K]^{-1}[B][C^{-1} + DK^{-1}B]^{-1}[D]\{x\} \quad (A.8)$$

The solution vector {x} (and, thus, {x + Δx}) chosen for the piping system is the vector of displacements of the swaybraces; since each swaybrace force is proportional to its displacement, the swaybrace forces are updated at each step--reanalysis plus application of each load increment--until all of the load has been applied.

A computer program was written to automatically increment the load at Node 101 X' (see figure in text) until a swaybrace changed stiffness from k_1 to k_2, and then to perform subsequent reanalysis to reflect the revised stiffness. This process was repeated until all of the 80-kN or 220-kN X' load was applied. Table A.1 depicts this process: shown is each load increment and the swaybraces which have changed to stiffness k_2. As seen from the table, nine of the twelve swaybraces were computed to have been in the k_2 stiffness region for application of the 80-kN load at Note 101 X'; for the 220-kN load, one additional swaybrace was in the k_2 stiffness region.

Swaybrace forces were computed by performing MSC/NASTRAN dynamic pseudoforce analyses for the 80-kN and 220-kN applied loads. Table A.2 presents a comparison between MSC/NASTRAN-computed and reanalysis-computed swaybrace forces. Both computations agree, which is further validation of the dyanmic pseudoforce method in general, and which is verification that the nonlinear swaybraces were correctly incorporated into the piping system model, in particular. Note that the dynamic pseudoforce method and nonlinear swaybrace modeling were verified by using a linear model in a piecewise linear fashion

TABLE A.1: PROGRESSION OF REANALYSIS PROCEDURE

Load Increment (N)	Cumulative Load (N)	Swaybraces with Stiffness k_2
11,647	11,647	—
7,305	18,952	4
1,204	20,156	4,14
5,170	25,326	4,8,14
19,175	44,501	4,8,13,14
2,194	46,695	4,8,9,13,14
5,498	52,193	3,4,8,9,13,14
70	52,263	2,3,4,8,9,13,14
17,360	69,623	2,3,4,7,8,9,13,14
10,377	80,000	2,3,4,6,7,8,9,13,14
122,797	202,797	2,3,4,6,7,8,9,13,14
17,203	220,000	2,3,4,6,7,8,9,11,13,14

TABLE A.2: STRUCTURAL REANALYSIS AND DYNAMIC PSEUDOFORCE COMPARISON

	Computed Swaybrace Forces (N)			
	80-kN force		220-kN force	
Swaybrace	Pseudoforce	Reanalysis	Pseudoforce	Reanalysis
1	115	97	-2678	-2701
2	2795	2827	3319	3482
3	-2797	-2829	-3298	-3441
4	3194	3313	4259	4616
5	1879	1849	1091	1144
6	2717	2746	3177	3372
7	-2751	-2774	-3278	-3389
8	3123	3228	4122	4476
9	-2723	-2739	-2848	-2889
11	-97	-115	-2708	-2722
13	2900	2957	3480	3671
14	2871	2919	3317	3463

to obtain the final results. The piecewise linear analysis could have been done with the linear MSC/NASTRAN model, though it would have required 11 separate computer runs, one for each piecewise linear incremental analysis. The reanalysis technique performed the same analyses, though in a much more efficient manner.

Dynamic Solution Benchmark--Complex Model

After the pseudoforce method was validated on simple problems, and after proper incorporation of the nonlinear swaybraces into the piping system model was verified, the 80-kN and 220-kN X' snapback tests were simulated. Validity of the computer-generated results is dependent upon the ability of the MSC/NASTRAN-implemented pseudoforce method to accurately simulate the desired nonlinear swaybrace force deflection characteristics.

Selected force-deflection curves for the 80- and 220-kN X' snapback simulations are shown in Figures A.6 and A.7. Figure A.8 shows similar plots with the desired force-deflection curve superimposed on each analytical curve. Note that the 80-kN simulation curves appear to follow the desired curve much better than do the 220-kN simulation curves. In fact, curves from the 220-kN simulation appear to exhibit significant hysteresis, even though the nonlinear swaybraces should be elastic. This hysteresis adds localized damping to the system, though it is probably an insignificant amount compared to the overall system damping.

The integration time step, Δt, is 0.005 s for both simulations. The 220-kN simulation was repeated with a time step of 0.0025 s; the force-deflection curves and acceleration peak values scarcely changed. Figure A.9 shows force-deflection curves for the two time steps. There were negligible acceleration changes from halving the time step, though force time histories did show significant differences. This is depicted in Figure A.10, which shows typical swaybrace force time histories for the two simulations; note

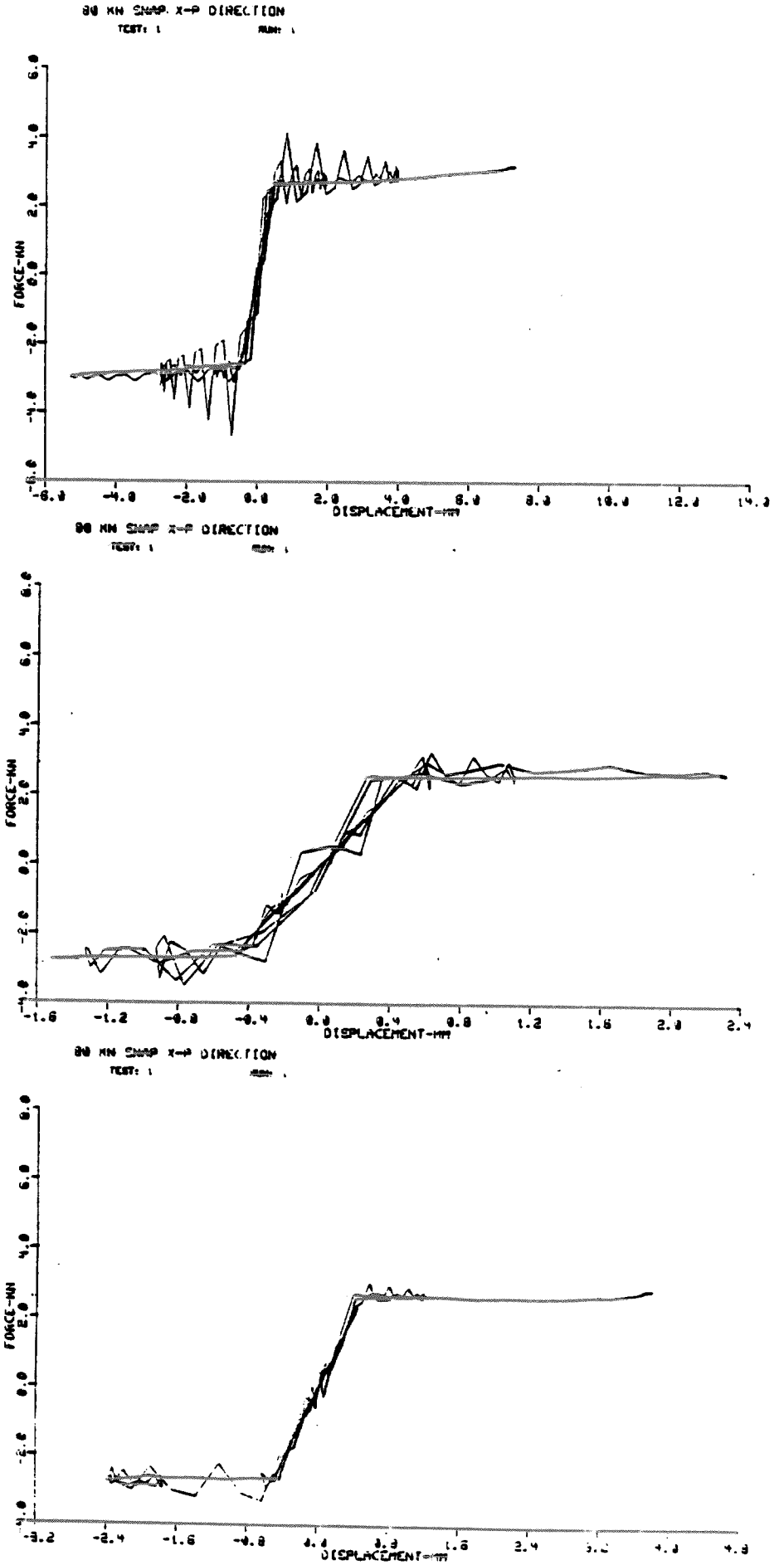

Figure A.6: Swaybrace Force-Deflection Curves--80-kN Snap

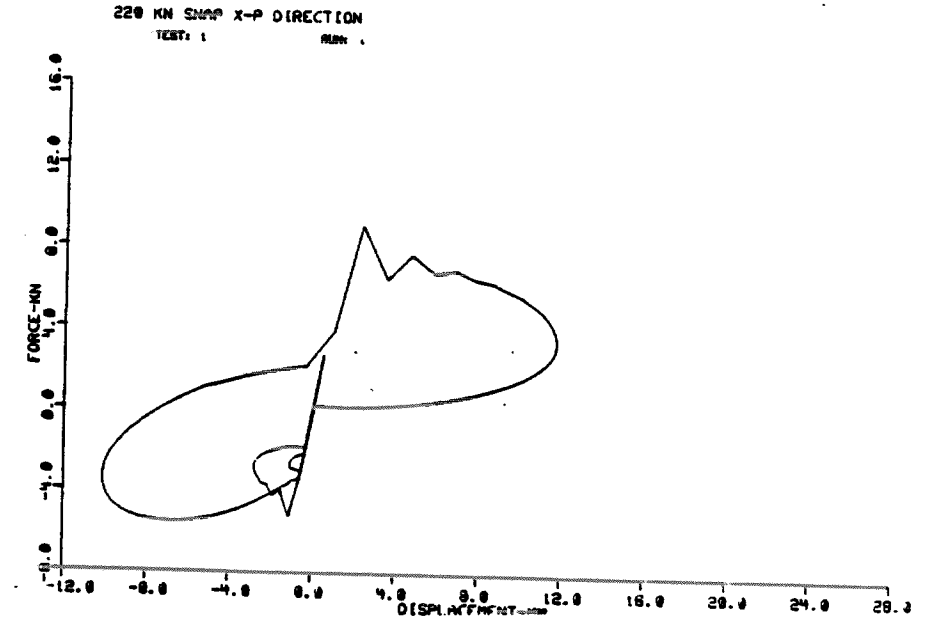

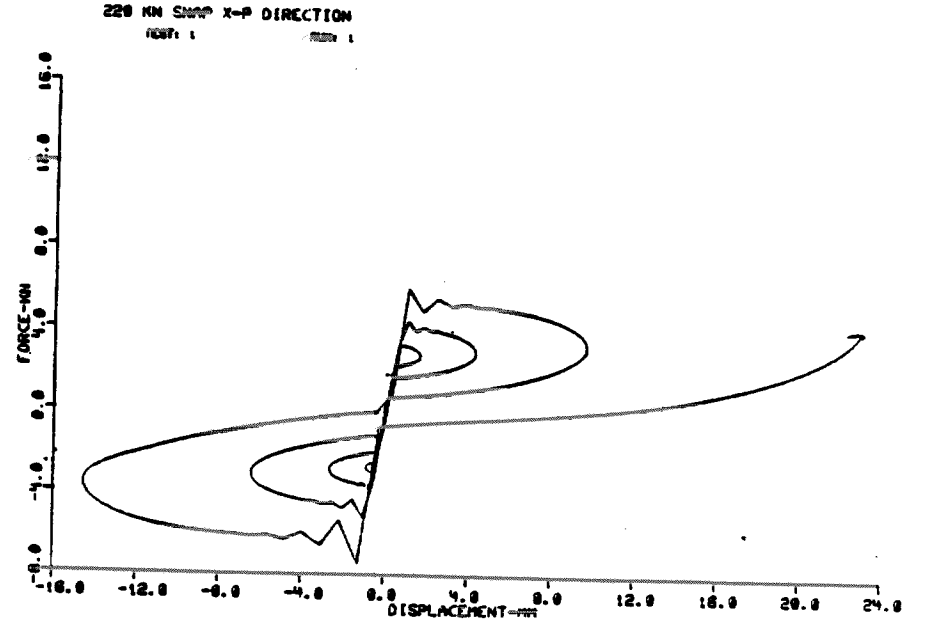

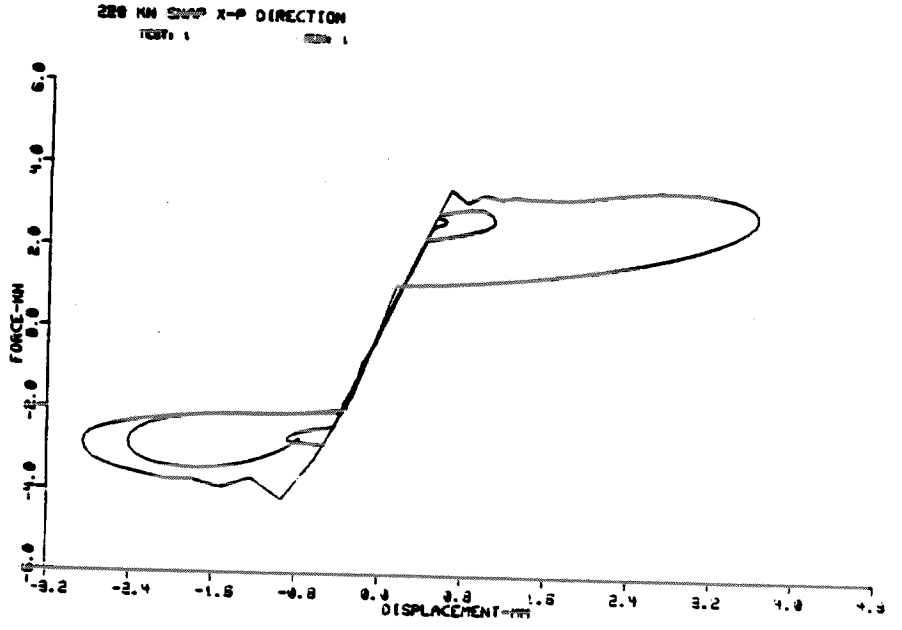

Figure A.7: Swaybrace Force-Deflection Curves--220-kN Snap

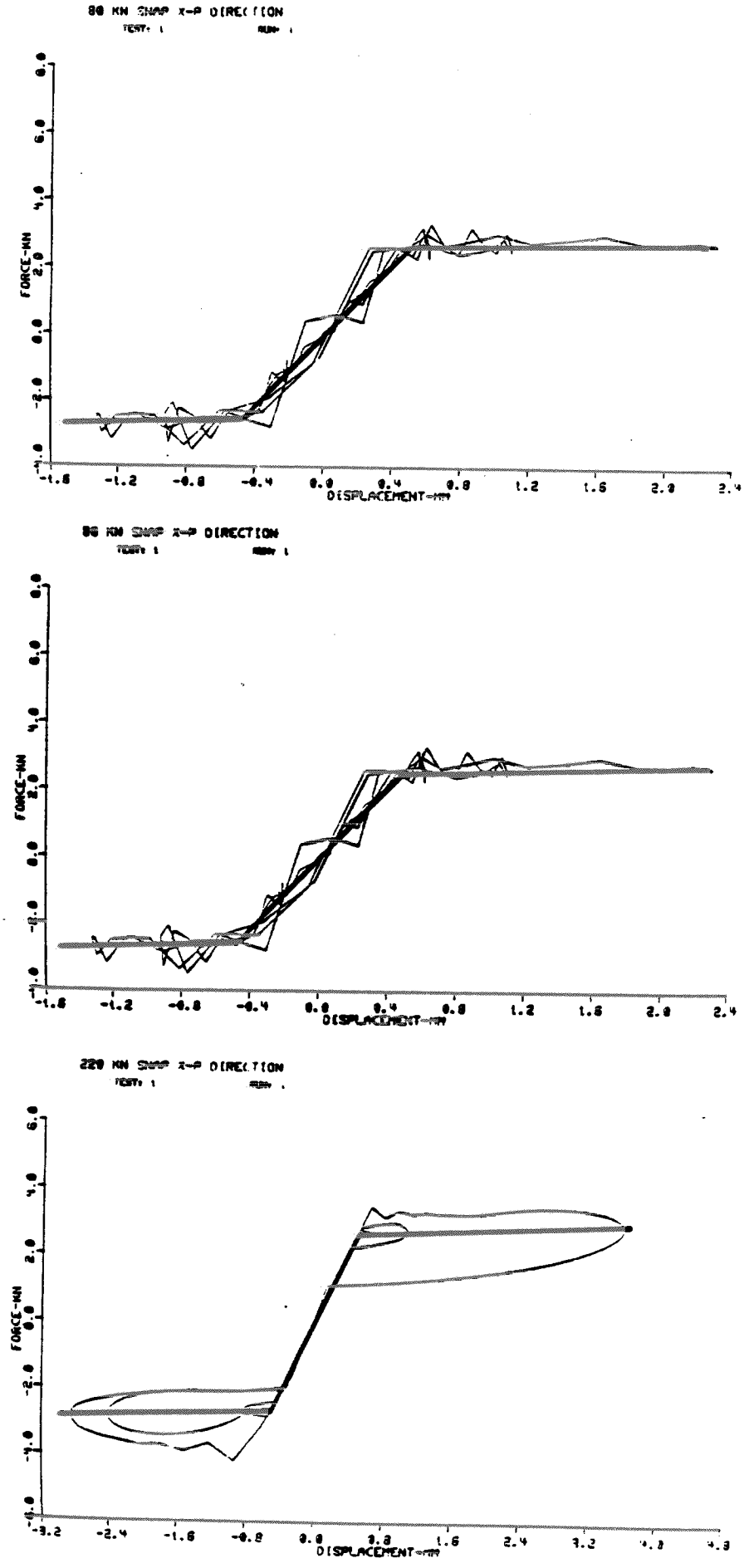

Figure A.8: Computed Force-Deflection Curves Compared to Ideal Curves

the response spike for the larger integration time step. This is due to the nonlinear force lagging the solution by an integration time step; this lag is more pronounced for the larger Δt. This decreased accuracy with increased Δt was also shown for the single degree-of-freedom system described earlier.

Swaybrace force-deflection curves were also computed for the seismic simulation. Since the grounded end of each swaybrace was stationary in the snapback simulations, each nonlinear force was calculated in terms of the absolute displacement of the unrestrained end of each swaybrace. This had to be changed for seismic excitation, since the grounded end of each swaybrace would undergo enforced motion. Therefore, relative displacement between the ends of each swaybrace was required, which necessitated the use of transfer functions and extra points. Representation of a single swaybrace with enforced motion at one end is shown in Figure A.11. The large-amplitude earthquake simulation was performed using direct integration with a time step of 0.005 s (the same as was used in the snapback simulations). Typical swaybrace force-deflection curves are shown in Figure A.12. Whereas these curves are not as accurate as those of the 80-kN snapback simulation, they are, nonetheless, better than the 220-kN snapback simulation curves. Particularly noticeable is the lack of apparent hysteresis, which--while perhaps not so important for the snapback simulations--is important for the seismic calculations.

Conclusions

This appendix described validation of the pseudoforce method and verification of proper nonlinear swaybrace incorporation into the piping system model. The integration time step was shown to be an important consideration in the pseudoforce method as implemented in MSC/NASTRAN. Further research is needed to formulate *a-priori* guidelines for integration step size as a function of system resonant frequencies, severity of nonlinearties, and type of applied loading.

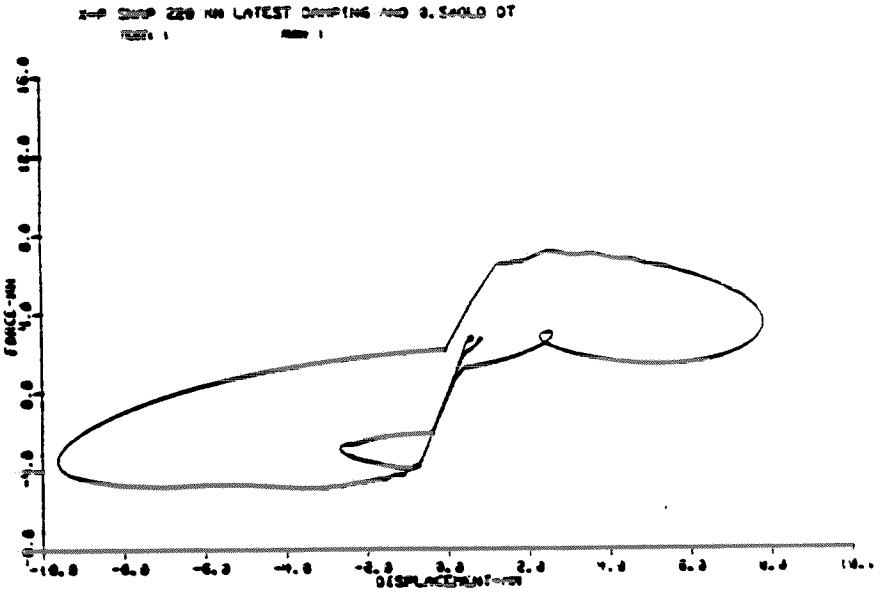

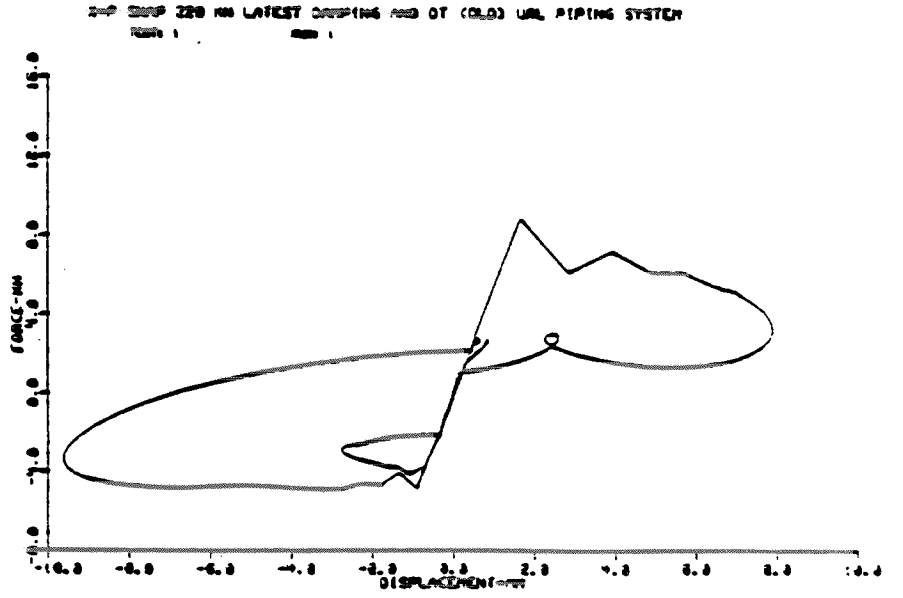

Figure A.9: Effect of Integration Time Step on Swaybrace Force-Deflection Curve--Piping System

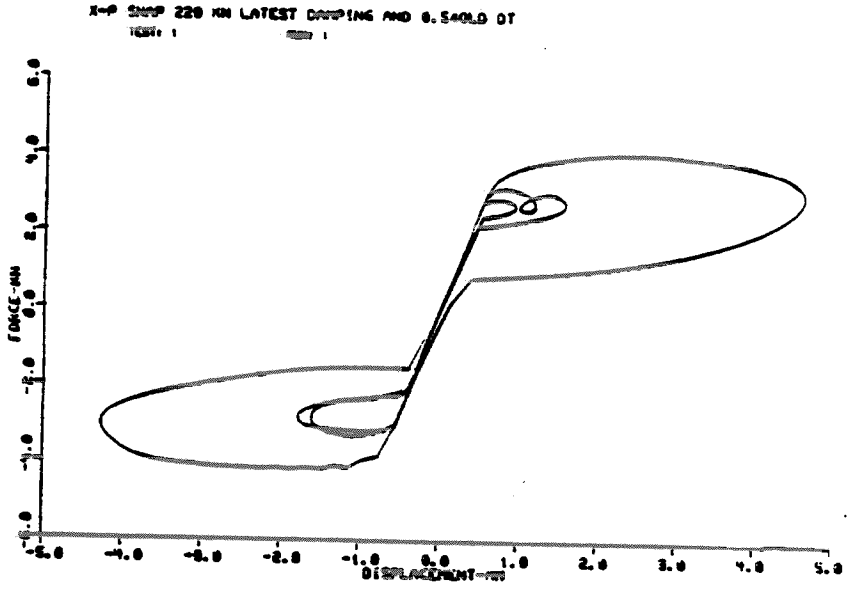

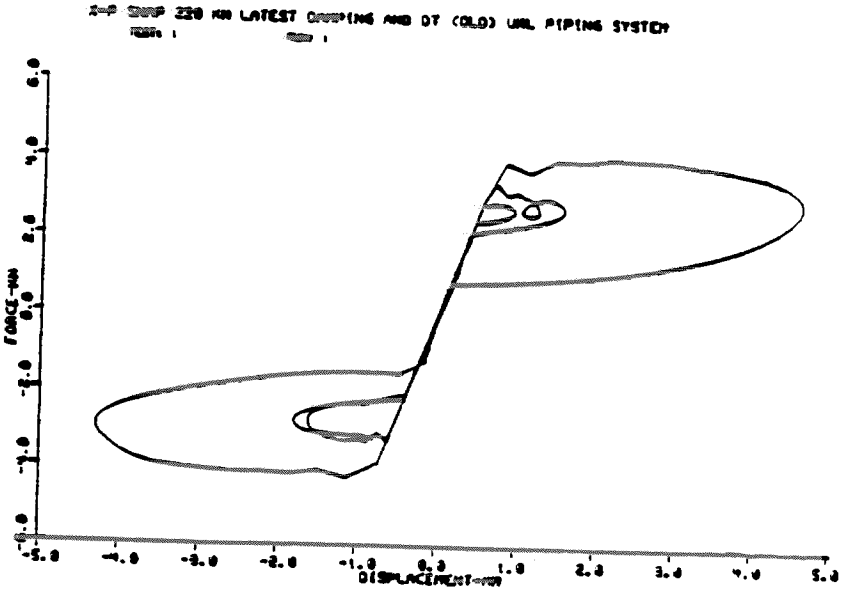

Figure A.9 (Continued)

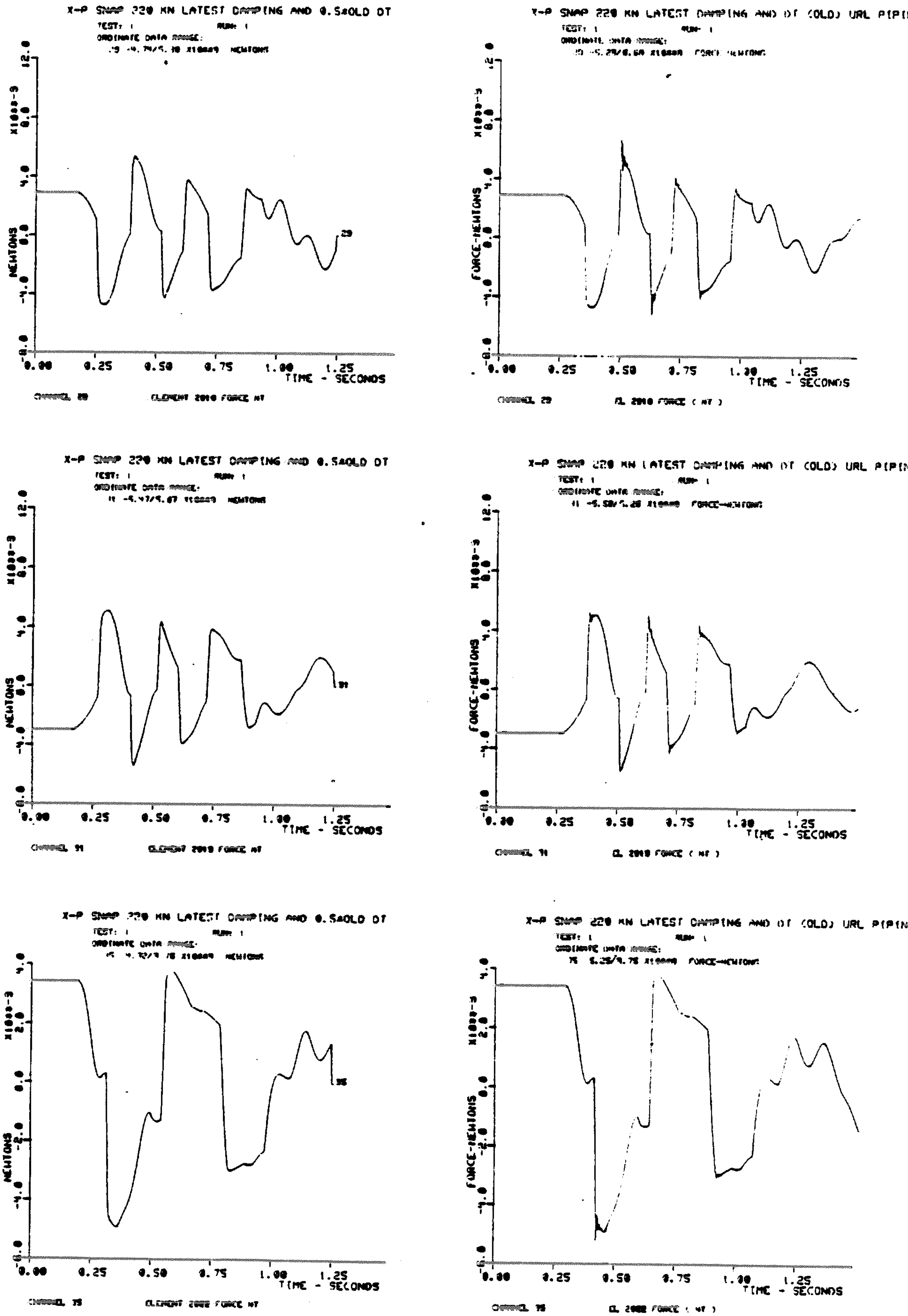

Figure A.10: Effect of Integration Time Step on Swaybrace Forces

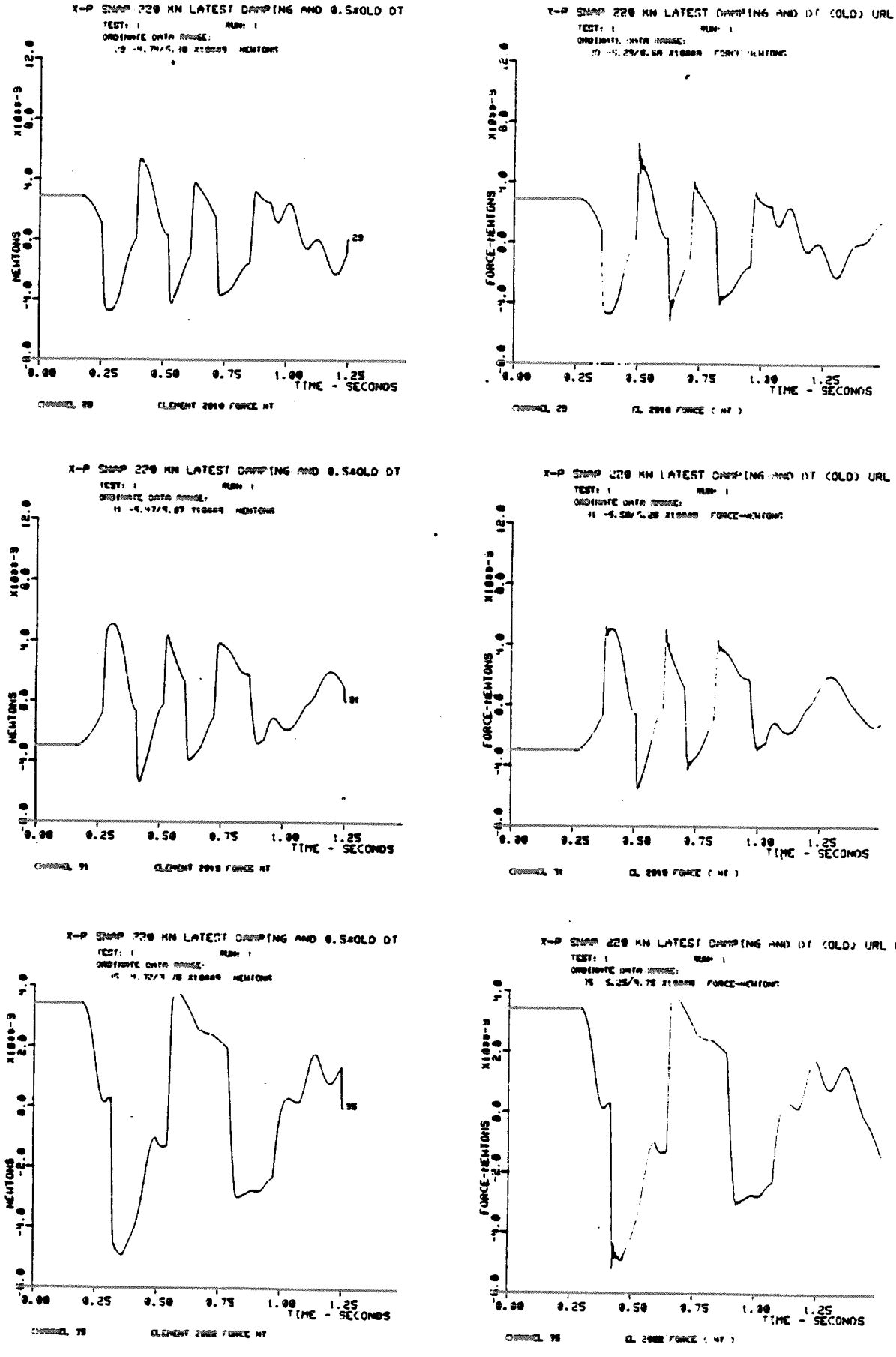

Figure A.10: Effect of Integration Time Step on Swaybrace Forces

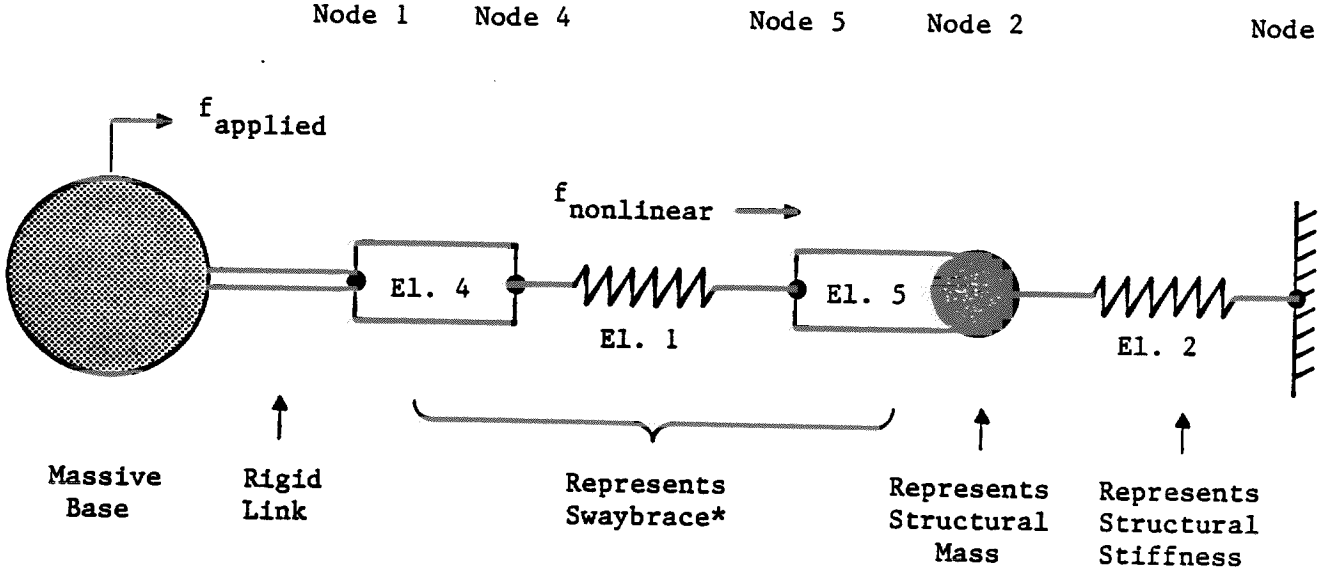

*Transfer function and extra point defined to represent relative displacement

Figure A.11: Representation of Single Swaybrace for Seismic Excitation

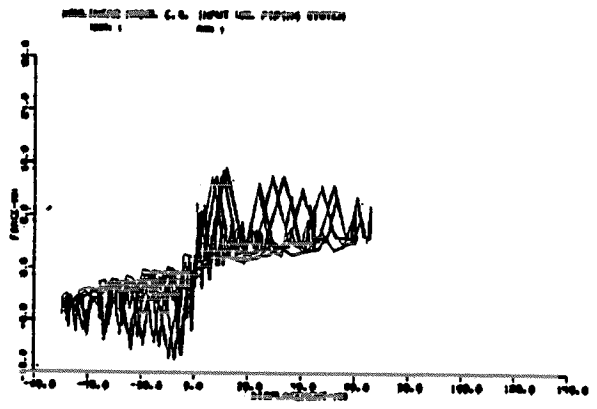

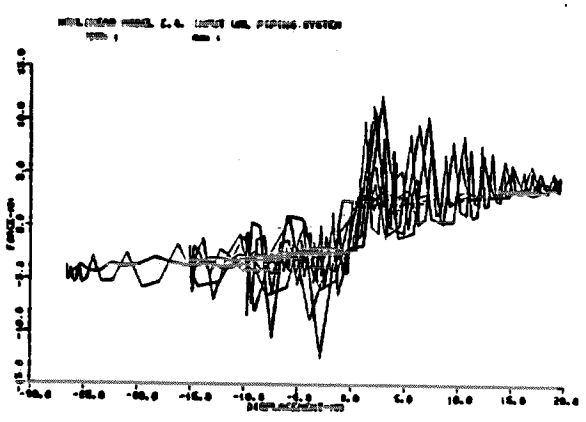

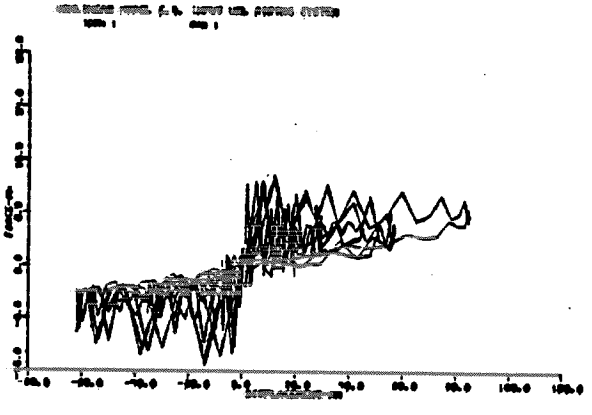

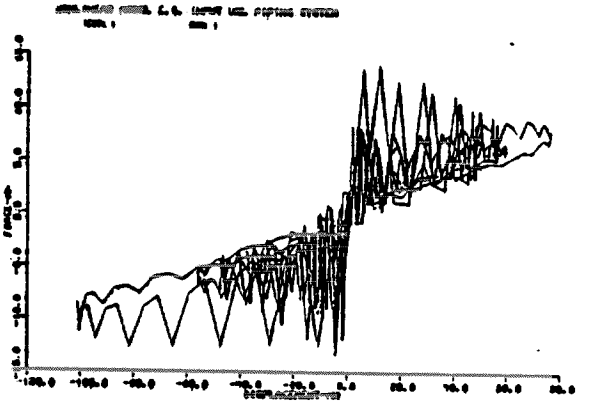

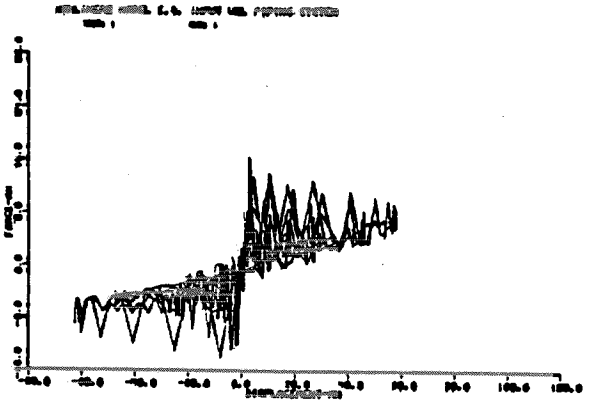

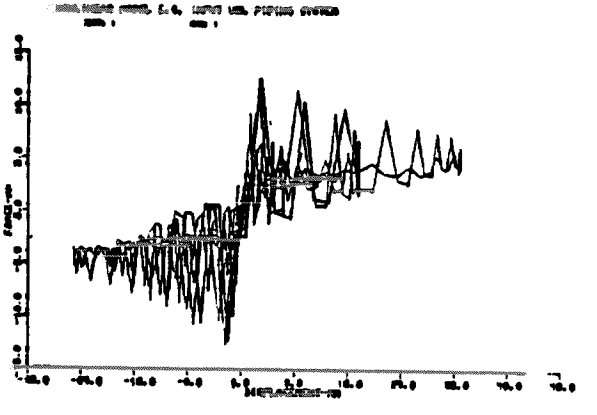

Figure A.12: Typical Swaybrace Force-Deflection Curves--Seismic Excitation

REFERENCES

A.1 J.S. Arora, "Survey of Structural Reanalysis Techniques," Journal of the Structural Division, ASCE, Vol. 102, No. ST4, April 1976, pp. 783-802.

A.2 K.D. Blakely, "Computational Techniques for Solving Systems with Large Stiffness Changes," Thesis, University of California, Los Angeles, CA, June 1981.

A.3 A.S. Householder, The Theory of Matrices in Numerical Analysis, Dover Publications, New York, NY, 1964.

A.4 B.P. Wang and W.D. Pilkey, "Efficient Reanalysis of Locally Modified Structures," Proc. First Chautauqua on Finite Element Modeling, Harwichport, MA, September 1980.